

Using aquaplanets to understand the robust responses of comprehensive climate models to forcing

Brian Medeiros · Bjorn Stevens · Sandrine Bony

Received: 3 December 2013 / Accepted: 6 April 2014
© The Author(s) 2014. This article is published with open access at Springerlink.com

Abstract Idealized climate change experiments using fixed sea-surface temperature are investigated to determine whether zonally symmetric aquaplanet configurations are useful for understanding climate feedbacks in more realistic configurations. The aquaplanets capture many of the robust responses of the large-scale circulation and hydrologic cycle to both warming the sea-surface temperature and quadrupling atmospheric CO₂. The cloud response to both perturbations varies across models in both Earth-like and aquaplanet configurations, and this spread arises primarily from regions of large-scale subsidence. Most models produce a consistent cloud change across the subsidence regimes, and the feedback in trade-wind cumulus regions dominates the tropical response. It is shown that these trade-wind regions have similar cloud feedback in Earth-like and aquaplanet warming experiments. The tropical average cloud feedback of the Earth-like experiment is captured by five of eight aquaplanets, and the three outliers are investigated to understand the discrepancy. In two models, the discrepancy is due to

warming induced dissipation of stratocumulus decks in the Earth-like configuration which are not represented in the aquaplanet. One model shows a circulation response in the aquaplanet experiment accompanied by a cloud response that differs from the Earth-like configuration. Quadrupling atmospheric CO₂ in aquaplanets produces slightly greater adjusted forcing than in Earth-like configurations, showing that land-surface effects dampen the adjusted forcing. The analysis demonstrates how aquaplanets, as part of a model hierarchy, help elucidate robust aspects of climate change and develop understanding of the processes underlying them.

Keywords Climate change · Climate models · Cloud radiative effect · Aquaplanet · Tropospheric adjustment · Climate feedbacks

1 Introduction

Comprehensive climate models encapsulate current knowledge of Earth's climate, and provide powerful tools for understanding the consequences of increasing greenhouse gas concentrations. Their complexity, however, makes it difficult to unravel the mechanisms of climate change. A hierarchy of models can be used to develop understanding in simpler contexts and connect to more complex systems (Bony et al. 2013b; Brient and Bony 2013). In the present case, we are motivated to better understand cloud feedbacks in climate models, since, as has been widely repeated, cloud feedbacks remain an important source of uncertainty in climate projections (Cess et al. 1989; Boucher et al. 2013).

The idealized experiments used here remove the ocean component of the models by fixing sea-surface temperature

Electronic supplementary material The online version of this article (doi:[10.1007/s00382-014-2138-0](https://doi.org/10.1007/s00382-014-2138-0)) contains supplementary material, which is available to authorized users.

B. Medeiros (✉)
National Center for Atmospheric Research,
PO BOX 3000, Boulder, CO 80307, USA
e-mail: brianpm@ucar.edu

B. Stevens
Max Planck Institute for Meteorology,
Bundesstr. 53, 20146 Hamburg, Germany

S. Bony
Laboratoire de Météorologie Dynamique, IPSL,
CNRS, Paris, France

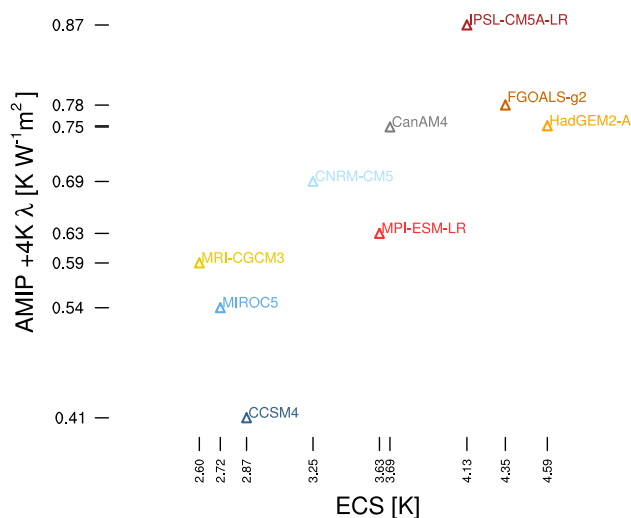


Fig. 1 Relationship between the AMIP global sensitivity parameter and equilibrium climate sensitivity inferred from coupled model experiments. *Colors* show the AMIP value of the tropical cloud effect parameter (see text); discrepancies between the *colors* and the *vertical position* show the influence of extratropical climate responses. Two models not included by Andrews et al. (2012) are added to Fig. 1: CCSM4 and FGOALS-g2 (see Table 1 for a list of models). Other results from those models are presented in the text, so the ECS was calculated as in Andrews et al. (2012) (using the method of Gregory et al. 2004). The CanAM4 results are presented in Fig. 1, but excluded from the remainder of this discussion because no aquaplanet results are available for that model

(SST) and sea-ice. The control simulations employ time-varying observed SST and sea-ice [in the spirit of, and named after the Atmospheric Model Intercomparison Project (AMIP), Gates 1992], and climate changes are prescribed by either uniformly increasing the SST by 4K or by quadrupling the atmospheric CO₂ concentration. We compare results from the AMIP experiments with further idealized aquaplanet versions of the same models and the same climate perturbations. The SST+4K warming experiments explore the climate response and associated climate feedbacks (in the absence of SST feedbacks) in analogy to a global warming scenario, as in Cess et al. (1989, 1990, 1996). Increasing atmospheric CO₂ provides insight into the tropospheric adjustment to the direct radiative forcing from CO₂ (Hansen et al. 2002; Gregory and Webb 2008).

The idealized warming experiments with the AMIP configuration capture much of the global response of the fully-coupled projections. This point is illustrated with the help of Fig. 1 which compares the global equilibrium climate sensitivity (ECS) for several ocean-atmosphere coupled models calculated by Andrews et al. (2012) with the climate sensitivity parameter (λ , defined by Cess et al. 1989) for the corresponding AMIP SST+4K experiments. This comparison confirms other recent findings that AMIP

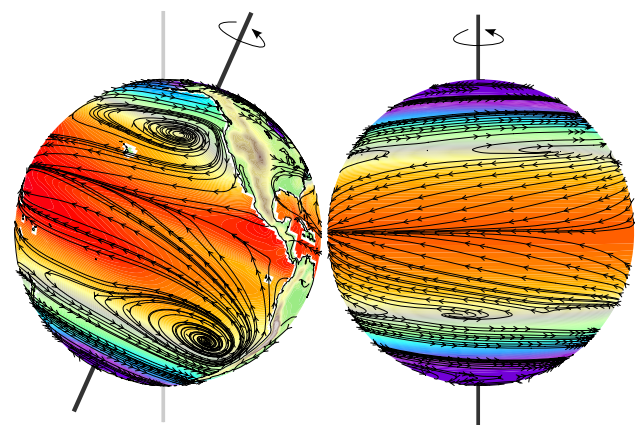


Fig. 2 Illustration of the *left* AMIP and *right* AQUA configurations. *Color shading* shows SST for ocean locations and topography for land locations; *streamlines* show the annual mean flow at 925 hPa

experiments contain similar feedbacks as experiments with fully-coupled climate models (e.g. Tomassini et al. 2013; Briant and Bony 2013).

Aquaplanets are an idealized configuration in which the planet's surface is completely water-covered. This simpler setting still allows a global model's explicit dynamics and parameterized physics to interact within an Earth-like climate. The configurations used here, illustrated by Fig. 2, are modeled after the AquaPlanet Experiment Project (APE, Neale and Hoskins 2000; Williamson et al. 2012). In particular, the SST is prescribed using a simple analytic profile (so-called "QOBS," maximum on the Equator reaching 0 °C at 60° latitude), sea-ice is neglected, and orbital parameters are defined as perpetual equinox conditions (i.e., there is no seasonality, but the diurnal cycle is retained). Aquaplanets are an attractive framework because they retain the dynamics and physics of more realistic configurations while eliminating zonal asymmetries and interactions with a more complex land-surface. Simplifying the lower boundary and orbital parameters, and hence reducing the dimensionality, provides a conceptually simpler configuration that facilitates analysis and allows shorter integrations. These potential advantages are valid for studies of both the mean climate and idealized climate change experiments. Such simplifications may, however, introduce differences from more realistic model configurations, and aquaplanet climate response might differ among models more than Earth-like configurations, for instance by accentuating certain biases. Blackburn et al. (2013) have highlighted that some aspects of aquaplanet simulations show more variation across models than Earth-like simulations, such as the structure of the ITCZ and tropical precipitation variability. In the climate change context, differences from the Earth-like configurations may

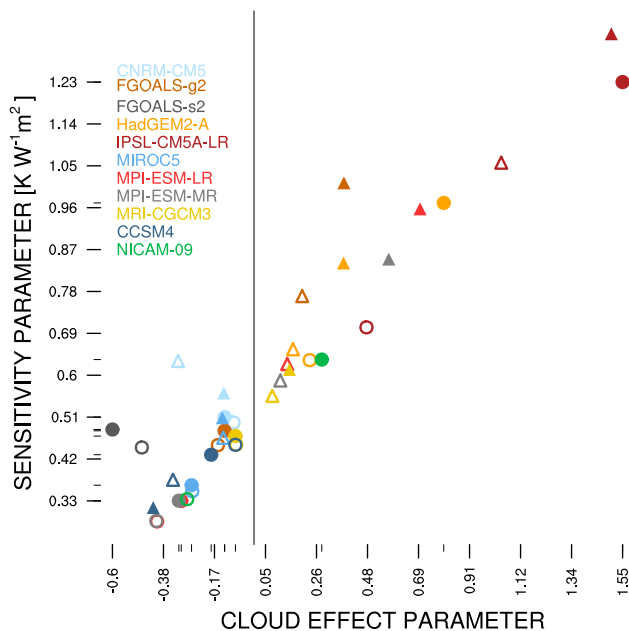


Fig. 3 Sensitivity versus cloud effect parameter for SST+4K warming experiments. *Triangles* show the AMIP experiments, *circles* show the aquaplanets. *Solid symbols* are the tropical values, while *unfilled symbols* are the global values. *Color* varies by model according to the AMIP tropical cloud effect parameter (i.e., *solid triangles* are ordered by *color horizontally*, cf. Table 1), except for the models in the lower part of Table 1 which are shown in *shades of gray* (FGOALS-s2, MPI-ESM-MR) and *green* (NICAM-09)

manifest because the Earth-like configurations contain a greater variety of states, so some regimes may not be well-sampled by aquaplanets. The present analysis explores these issues by investigating the extent to which aquaplanet climate change experiments capture aspects of the AMIP experiments.

Figure 3 presents the climate sensitivity parameter and a measure of the cloud response (called the cloud effect parameter and defined later) for all the SST+4K experiments, both globally and tropically. The symbols show the AMIP (triangles) and aquaplanet results (circles, hereafter abbreviated as AQUA), and colors differentiate each model by the AMIP tropical cloud effect parameter (that is, colors sort the solid triangles horizontally). The figure recalls the results from previous comparisons (e.g., Cess et al. 1989), showing the strong linear relationship between the overall sensitivity to warming and changes in cloud radiative effects. By definition, a linear relationship is expected, but the figure shows the surprisingly predictive power of cloud changes for the complete climate change. There is also a degree of agreement between AMIP and AQUA sensitivity, though three models have positive cloud effect parameters in the AMIP experiment but negative in the AQUA experiment.

Figures 1 and 3 demonstrate the usefulness of AMIP warming experiments for understanding fully-coupled

climate projections, that this response (in the tropics) is tightly linked to the cloud response, and that aquaplanets may capture important aspects of this tropical cloud response. Simplifying the system allows a critical view into the processes responsible for the response to climate perturbations. When the response of the simplified system mimics the more comprehensive system, it allows for an unobstructed analysis of the response. When the simplified system responds differently, it exposes the importance of representing those processes or features that are not present in the simplified system.

In the following, we ask whether the AQUA experiments offer a useful analogy to the AMIP configuration as a framework for simplifying and understanding climate response to perturbations. We start in Sect. 2 with some comments on the included models and the general approach to the analysis. In Sect. 3 we show similarities and differences between the AMIP and AQUA experiments in the distribution of atmospheric states, and show that the tropical circulation and hydrologic cycle exhibit some robust responses across models in both configurations. Section 4 examines the cloud response to warming, and Sect. 4.1 focuses on three models that exhibit discrepancies between configurations. The tropospheric adjustment to quadrupling CO₂ is explored in Sect. 5.

2 Models, experiments, and methods

2.1 Models

Table 1 lists the models used. The models in the upper part of the table are relatively independent and contain all necessary output information required for analyses herein. The models in the lower part of the table are missing some simulations that are necessary for the present analysis. The exception is the MPI-ESM-MR which is considered redundant because it differs from MPI-ESM-LR only through higher resolution in the upper troposphere and stratosphere and slight changes in the land mask associated with a different ocean grid (Stevens et al. 2013); these differences are minimal for our purposes. The choice of models depended on availability from the CMIP5 archive at time of writing. Also listed in Table 1 are the grid sizes of each model, the tropical (35°S–35°N) sensitivity and cloud effect parameters for the SST+4K experiments, and the cloud effect parameter for the 4 × CO₂ experiment (in which sensitivity is near zero because the sea surface temperature change is kept unchanged, see Sects. 2.2, 5). The pragmatic definition of the tropics (35°S–35°N) is chosen to capture the full Hadley circulation in all the simulations, and as shown below (Fig. 5) this approximation works for the present purposes, but extratropical

Table 1 The models examined in this study, with their grid sizes, tropical sensitivity and cloud effect parameters

Model	Center	Grid Size [LAT × LON × LEV]	+4K λ [K W ⁻¹ m ²]		+4K Δ CRE/G		4 × CO ₂ Δ CRE/G	
			AMIP	AQUA	AMIP	AQUA	AMIP	AQUA
CCSM4	NCAR, USA	192 × 288 × 26	0.33	0.45	−0.34	−0.20	−0.16	0.0002
CNRM-CM5	CNRM/CERFACS, France	128 × 256 × 31	0.60	0.51	−0.07	−0.12	0.003	0.06
FGOALS-g2	LASG-CESS, China	60 × 128 × 26	0.99	0.48	0.47	−0.12	−0.06	−0.12
HadGEM2-A	MOHC, UK	145 × 192 × 38	0.87	0.97	0.40	0.80	0.10	−0.02
IPSL-CM5A-LR	IPSL, France	96 × 96 × 39	0.93	1.23	0.79	1.55	0.14	0.15
MIROC5	MIROC, Japan	128 × 256 × 40	0.54	0.36	−0.09	−0.26	−0.03	−0.08
MPI-ESM-LR	MPI-M, Germany	96 × 192 × 47	0.88	0.33	0.53	−0.31	−0.02	−0.22
MRI-CGCM3	MRI, Japan	160 × 320 × 35	0.64	0.47	0.16	−0.08	0.11	0.02
CanAM4	CCCma, Canada	64 × 128 × 35	0.74	–	0.28	–	0.04	–
FGOALS-s2	LASG-IAP, China	108 × 128 × 26	–	0.48	–	−0.60	–	0.13
MPI-ESM-MR	MPI-M, Germany	96 × 192 × 95	0.79	0.33	0.43	−0.32	−0.01	−0.17
NICAM-09	NICAM Group, Japan	1280 × 2560 × 40	–	0.63	–	0.28	–	−0.59

The surface temperature is used, except for NICAM-09 which uses the near-surface temperature; using near-surface temperature slightly increases the sensitivity, on average by 0.01 K W⁻¹ m². For the AMIP experiments, land has not been removed from these averages. Dashes mark values that can not be calculated due to incomplete data

influences are included in tropical averages, especially for the AQUA configurations. Using 30° produces the same qualitative results as those presented.

The CMIP5 AMIP simulations are driven by observed SST and sea-ice over the period 1979–2008 (some models include years beyond these bounds, and we simply include those years here). The AQUA simulations are 5 years long and follow the APE protocol as outlined by Neale and Hoskins (2000). Most of the models used the “QOBS” SST distribution, but MIROC5 and FGOALS-g2 were run with the “CTRL” distribution. The latter has steeper meridional SST gradients, favoring a more equatorial ITCZ. While Medeiros et al. (2008) suggest such differences in the circulation do not strongly impact the climate response, we keep this difference in mind in the following analysis, cognizant of recent findings that show the SST profile acts as a control on boundary layer moist static energy and hence the position and structure of the tropical rain bands. (Moebis and Stevens 2012; Oueslati and Bellon 2013).

Not only does the FGOALS-g2 AQUA simulation use a different SST pattern, but “ghost” continents appear in some of the shortwave radiation fields. Excluding the “continents” does not qualitatively impact results. The FGOALS-s2 AQUA simulations have the same shortwave artifacts, but uses the standard “QOBS” SST distribution. The AMIP experiments are not available for the FGOALS-s2, but are expected to be similar to FGOALS-g2 as the two models differ only in their choice of dynamical core (Lin et al. 2013).

The NICAM-09 is a global cloud-system resolving model with grid spacing of about 14 km (Satoh et al. 2008; Yoshizaki et al. 2012). Due to the computational expense

of running at such high resolution, its simulations are much shorter than the other models (90 days for the control and SST+4K, 30 days for 4 × CO₂) and have no spin up period preceding the archived output. The 4 × CO₂ simulation also includes the SST warming. Because of the relatively low signal to noise in these experiments, along with the lack of corresponding AMIP experiments, we present limited results from NICAM-09. Those results discard the first month of output when possible to reduce initial noise, and when applicable the northern and southern hemispheres are averaged to decrease noise.

Throughout this analysis, monthly mean fields are used. When monthly fields are not available from the CMIP5 archive, they are constructed from higher frequency output.

2.2 Approach

Using idealized climate change experiments such as prescribed SST warming or quadrupling CO₂ simplifies the usual climate change analysis. A typical starting point for understanding climate change is through the global average energy balance at the top-of-atmosphere (TOA). A change in the radiative forcing, F , is accompanied by a change in the TOA radiative flux, R , until the system returns to equilibrium and the radiative perturbation vanishes ($\Delta R = 0$). To measure the response, usually the globally averaged surface temperature, T , is used along with a feedback parameter, λ . Combining these: $\Delta R = F + \lambda \Delta T$. The feedback parameter encapsulates a number of processes, including a Planck response and albedo, water vapor, lapse rate, and cloud feedbacks. While equilibrium climate change experiments make use of $\Delta R = 0$, the

idealized experiments discussed here turn the tables, equating ΔR to either the response or the forcing. In the SST warming experiments, ΔT is the prescribed climate change, and no external forcing is applied ($F = 0$), leaving $\Delta R = \lambda \Delta T$, and λ is defined here as the sensitivity parameter (following Cess et al. 1989, see Fig. 3). In $4 \times \text{CO}_2$ experiments $\Delta T = 0$, and the TOA radiative imbalance is the forcing, $\Delta R = F$, but including not only the instantaneous effect of CO_2 on radiative transfer, but the rapid adjustments in the rest of the system (see, e.g., Gregory et al. 2004; Gregory and Webb 2008). Because it contains these rapid adjustments, in this context F is often referred to as the adjusted forcing.

To measure the cloud response, we employ the cloud radiative effect (CRE). This is calculated by differencing the TOA net downward radiative flux in all-sky versus clear-sky conditions, $\text{CRE} \equiv R - R_{\text{clr}}$, which is accomplished in climate models by repeating the radiative transfer calculation excluding clouds. The CRE response, ΔCRE , is an estimate of the effect that cloud changes have on the TOA radiative fluxes. It is important to bear in mind that inclusion of clear-sky fluxes in the definition of CRE can affect ΔCRE through non-cloud changes (such as shortwave effects of surface albedo changes, or longwave effects of changes in CO_2 , Soden et al. 2004; Zelinka et al. 2013). Despite this shortcoming, several studies have shown that ΔCRE is closely related to more direct measures of cloud feedback (Soden et al. 2004; Vial et al. 2013). Because it is simpler to estimate and it proves to be a good predictor of the feedback factor, particularly at low latitudes where model differences are more decisive (e.g., Vial et al. 2013), ΔCRE is used in the present study to measure cloud feedbacks. The cloud effect parameter used above is defined as $\frac{\Delta \text{CRE}}{\Delta R}$ and is determined mainly by the CRE response.

Previous work with aquaplanet configurations have shown similarities to more realistic configurations (Medeiros et al. 2008; Brient and Bony 2012; Bony et al. 2013a; Medeiros and Stevens 2011), and implied that the aquaplanet configuration is therefore useful for understanding aspects of the mean tropical climate and its response to climate perturbations. The broad averages of Fig. 3 appear to indicate that this conclusion holds across a larger ensemble of models. The similarity between AQUA and AMIP simulations can be extended to the regional scale by conditioning on dynamic regimes (e.g., Medeiros and Stevens 2011).

Much of the variation among model estimates of climate sensitivity derives from differing cloud responses (Fig. 3). A framework for understanding such changes was introduced by Bony et al. (2004), in which a variable describing the large-scale state, \mathbf{x} , is used to decompose a cloud-related variable, c , with the mean value of c given by

$$\bar{c} = \int c(\mathbf{x}) \mathbf{P}(\mathbf{x}) d\mathbf{x} \quad (1)$$

Here $\mathbf{P}(\mathbf{x})$ is the statistical weight of each regime, which is the same as the relative area covered by each regime in each month. The response is then written and abbreviated as

$$\begin{aligned} \Delta \bar{c} &= \int \Delta c(\mathbf{x}) \mathbf{P}(\mathbf{x}) d\mathbf{x} \\ &+ \int c(\mathbf{x}) \Delta \mathbf{P}(\mathbf{x}) d\mathbf{x} + \text{higher order terms} \\ &= \mathcal{T} + \mathcal{D} + \mathcal{R} \end{aligned} \quad (2)$$

The Δ denotes the change with respect to the control climate. The first term on the rhs is called the thermodynamic contribution to the change and the second is the dynamic contribution; \mathcal{R} denotes residual terms (i.e., co-variation terms) that tend to be small. The thermodynamic contribution is due to changes in cloud properties within a given regime, while the dynamic term measures the change in the statistical weight of each regime. The clearest expression of an aquaplanet capturing the response of the Earth-like configuration is then, $\Delta \bar{c}_{\Delta} = \Delta \bar{c}_{\text{O}}$, where we adopt subscript triangles for the Earth-like AMIP configurations which contain continents and topographic features like mountains and subscript circles for AQUA configurations which are devoid of surface features (we also employ this convention in the figures). When averaged over the tropics, the dynamic contribution averages nearly to zero, which can be shown to be a consequence of mass conservation and \bar{c} varying no more than linearly in \mathbf{x} . This leaves $\Delta \bar{c} \approx \mathcal{T}$, so we expect that $\Delta \bar{c}_{\Delta} \approx \mathcal{T}_{\Delta}$ and $\Delta \bar{c}_{\text{O}} \approx \mathcal{T}_{\text{O}}$, leaving the best case scenario for the aquaplanet to predict the Earth-like response as $\mathcal{T}_{\Delta} \approx \mathcal{T}_{\text{O}}$.

As discussed above, a useful measure of clouds is CRE, which we identify with c in Eqs. (1) and (2). Cloud amount, cloud-top height, and CRE correlate well with vertical motion, which motivated Bony et al. (2004) to use mid-tropospheric vertical velocity, ω_{500} , as the dynamic variable (\mathbf{x}); this approach has been followed in subsequent studies, and we continue to use it here. Although ω_{500} successfully separates deep convective regimes from subsidence regimes, within subsidence regimes cloud types are better separated by lower-tropospheric stability ($\text{LTS} \equiv \theta_{700} - \theta_{\text{sfc}}$), particularly in the tropics (e.g., Slingo 1987; Klein and Hartmann 1993; Medeiros et al. 2008; Medeiros and Stevens 2011). This is evident in the multimodel joint histograms of LTS and ω_{500} (Fig. 4, top panels).

Medeiros et al. (2008) argued that $\mathcal{T}_{\Delta} \approx \mathcal{T}_{\text{O}}$ for two resolutions of the NCAR CAM3 and the GFDL AM2, but noted some differences within subsets of regimes (in which both \mathcal{T} and \mathcal{D} matter). The conclusion in that case is that

Table 2 Tropical circulation intensity (hPa day^{-1}), defined as $I \equiv \hat{\omega}^\downarrow - \hat{\omega}^\uparrow$ where $\hat{\omega}^\downarrow$ is the tropical average of the downward $\hat{\omega}$, the vertically averaged vertical velocity (between 1000 and 100 hPa), and $\hat{\omega}^\uparrow$ is the average for upward values (Bony et al. 2013a)

Model	AMIP			AQUA		
	Control	+4K	$4 \times \text{CO}_2$	Control	+4K	$4 \times \text{CO}_2$
CCSM4	37.78	37.20	36.55	34.31	30.96	34.97
CNRM-CM5	41.12	40.04	39.77	34.63	32.31	34.02
FGOALS-g2	45.58	43.37	44.47	49.58	46.09	47.95
HadGEM2-A	47.55	45.45	45.49	59.06	53.20	57.35
IPSL-CM5A-LR	35.46	34.05	33.97	32.84	30.24	32.79
MIROC5	39.86	38.18	38.94	55.80	49.70	56.25
MPI-ESM-LR	45.38	44.66	44.50	50.47	58.30	50.60
MRI-CGCM3	45.81	45.18	43.85	50.72	50.41	48.60

Averages taken over ocean grid points only. For comparison, the ERA-Interim circulation intensity is $37.99 \text{ hPa day}^{-1}$ (Jan 1979–May 2011)

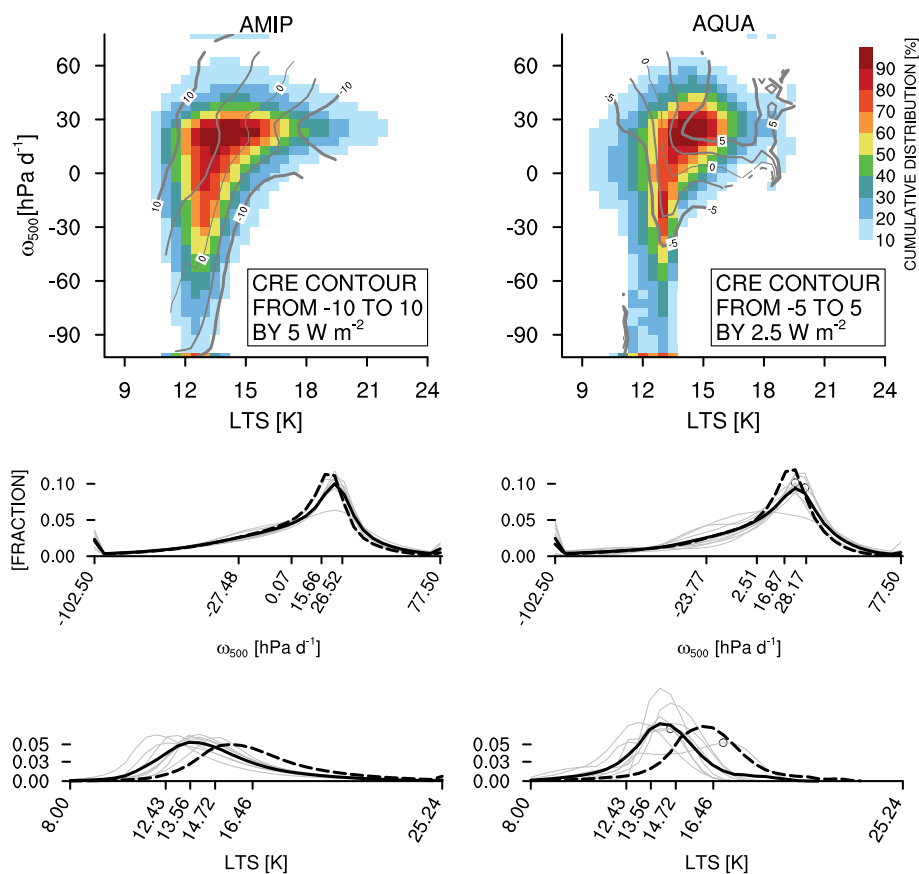


Fig. 4 Top row multimodel composite joint histogram of LTS and ω_{500} . Color intervals each encompass 10 % of the tropical data, determined by constructing the cumulative distribution from the joint histogram sorted in ascending order. The AMIP control simulations on the left, aquaplanet control simulations on right. Contour lines show the anomalous CRE, $\text{CRE}'(\text{LTS}, \omega_{500}) = \text{CRE}(\text{LTS}, \omega_{500}) - \text{CRE}$ where CRE is the tropical average CRE for an individual simulation, averaged over all models; intervals slightly differ to accommodate the reduced variability in the aquaplanet composite (see

labels). Middle row distribution of tropical ω_{500} , multimodel mean shown as dark, solid line. The multimodel mean for the SST+4K configuration shown in dark, dashed line. Individual models (control simulation) shown by thin, gray lines. Two small dark circles show the modes of the models with the steeper SST profile (CTRL rather than QOBS). Ticks along the horizontal axis mark extremes and quintile values of the multimodel mean of the control simulations. Bottom row as in middle row, but for the lower-tropospheric stability in subsidence regimes

the simpler aquaplanet provides a good laboratory to understand the mechanisms of the cloud response in more complicated model configurations. Even in the case $\mathcal{T}_\Delta \neq \mathcal{T}_\odot$, however, the aquaplanet is instructive because it can help identify which details of the model configuration (lower boundary condition, land–atmosphere interaction) lead to important aspects of the tropical climate response (asymmetric circulation response, or cloud coupling to asymmetries in the sea-surface temperatures).

3 Circulation response

This section explores the circulation and hydrologic responses of the AMIP and AQUA configurations to the imposed climate perturbations, and establishes the foundation for the dynamical regimes analysis.

To begin applying the approach described in Sect. 2.2, we investigate the distributions of the primary (ω_{500}) and secondary (LTS) control variables. The ensemble mean joint distribution is shown in Fig. 4. The joint distribution for the AMIP and AQUA configurations are similar in the upwelling regions of the tropics ($\omega_{500} < 0$), but differ in the subsiding regions. The AMIP configurations show an extension to higher LTS that is largely absent in the AQUA configurations. Both distributions are centered on weak subsidence and LTS, emphasizing the broad trade-wind regions of the tropical oceans. Figure 4 makes it apparent that stratifying the tropical atmosphere by ω_{500} separates deep convective regimes and their high-level cirrus clouds from subsidence regimes with low-level clouds under mostly clear skies, and thus provides a basis for a dynamical regimes decomposition. The ω_{500} distributions among the models (Fig. 4, middle panels) further indicate that the AMIP and aquaplanet tropics have similar Hadley circulations (see also Fig. 5). The multi-model distributions from the SST+4K simulations (dashed curves) show a narrowing of the distribution in both configurations as the dominant subsidence regime becomes associated with weaker subsidence and regions of extreme subsidence become less favored.

Figure 5 shows the Hadley circulation width and strength in each simulation; determined as the latitude where the zonal mean meridional streamfunction reaches zero and the maximum (absolute) value on either side of the equator (as in Gastineau et al. 2011). The narrowing of the ω_{500} distribution in the SST+4K experiment is part of an overall weakening and widening of the Hadley circulation with warming. This is a robust signal among the models for both the AMIP and AQUA configurations, and has been discussed widely using observations and models (see the review of Lucas et al. 2014). The AQUA configurations differ from the AMIP configurations in that they

consistently have narrower and stronger Hadley circulations. Despite the difference in size and strength, the AQUA experiments depict similar weakening and widening Hadley cells with warmer SST. The magnitude of weakening varies among the models, and the spread is dominated by variation in changes of the monthly mean upward motion. The only exception to the weakening signal is the MPI-ESM-LR AQUA which has a slight strengthening, suggesting a relatively disruptive circulation response to warming. The vigor of the tropical overturning circulation is further quantified by the circulation intensity diagnostic in Table 2 (following Bony et al. 2013a), which is consistent with Figure 5.

Diagnostics of the eddy-driven jet stream position and intensity are shown in Fig. 6. As with the Hadley circulation, the zonal circulation in the AQUA configurations is (generally) more intense than the AMIP simulations, and the AQUA jets are more equatorward than in the AMIP configuration. Seasonal effects are not shown, but can be substantial in the AMIP simulations. Under SST warming the eddy-driven jet shows a poleward migration for all the AQUA simulations and all AMIP southern hemispheres; the northern hemisphere is more varied due to strong zonal asymmetries and seasonal effects (see also Kidston and Gerber 2010; Barnes and Polvani 2013). A discrepancy between AMIP and AQUA is seen in the eddy-driven jet intensity change with warming: the AMIP experiments show a robust intensification, but the AQUA experiments show a robust weakening. One contributing factor to this difference may be the interaction of the eddy-driven and subtropical jets, which are difficult to distinguish in the aquaplanets (Lu et al. 2010). Examination of the upper-level zonal wind maxima, which are likely more strongly linked to the subtropical jet, produce AQUA results exhibiting an intensification and no poleward shift (not shown). The complications of separating the subtropical and eddy-driven jets thus make comparing the extratropical circulation response ambiguous, but the tropical circulation appears to respond similarly between the AMIP and AQUA configurations.

Figures 5 and 6 also document circulation changes with quadrupling CO_2 with fixed SST. As with warming, the AQUA responses generally mirror the AMIP experiments. In this case, the change in atmospheric opacity reduces infrared cooling and slightly stabilizes the troposphere, leading to a slight widening and weakening of the Hadley circulation. These changes are smaller than in the SST+4K case, and smaller in the AQUA than AMIP experiments. Table 2 shows that several AQUA experiments have a (negligibly) small increase in the circulation intensity; this discrepancy between the AMIP and AQUA experiments shows the influence of warming continents on the tropical circulation. The table also shows that the response to

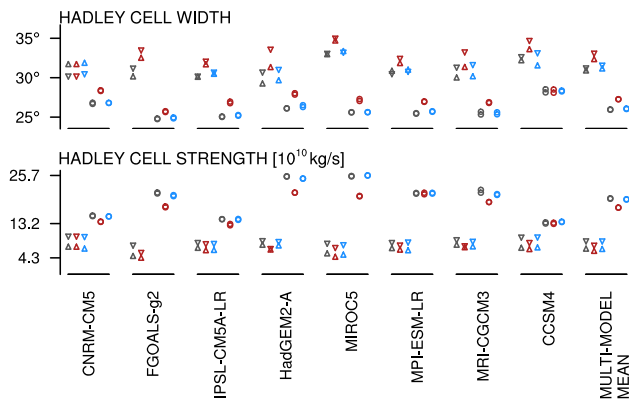


Fig. 5 Hadley circulation width (*top*) and strength (*bottom*) for each model and the multi-model mean (*far right*). Triangles denote the AMIP simulations (*upward* and *downward* pointing for northern and southern hemisphere, respectively) and circles the AQUA simulations. Gray markers show the control simulations, red the SST+4K, and blue the $4 \times \text{CO}_2$. The diagnostics are calculated using the meridional mass stream function vertically integrated between 700 and 300 hPa, $\hat{\psi}$. The width is determined as the most equatorward latitude where $\hat{\psi} = 0$ in each hemisphere, conditioned on being poleward of the absolute hemispheric maximum, $\hat{\psi}_{\text{MAX}}$, which defines the Hadley cell strength

quadrupling CO_2 is more robust than the response to SST warming (the spread among experiments is smaller) in both AMIP and AQUA experiments. The AMIP southern hemisphere has a slight poleward shift and intensification of the eddy-driven jet while the northern hemisphere shows a similar poleward shift but a weakening. The AQUA eddy-driven jets show a slight poleward migration and nearly no change in intensity.

The hydrologic cycle is closely connected to the large-scale circulation (Chahine 1993; Stevens and Bony 2013), and Figure 7 shows that aspects of the tropical hydrologic cycle also show robust responses in these experiments. Warming induces an increase in column-integrated water vapor (at a rate of around $7\% \text{ K}^{-1}$ following the temperature dependence of saturation specific humidity), and precipitation also increases but at a slower rate (around $2\text{--}3\% \text{ K}^{-1}$, cf., Mitchell et al. 1987; Held and Soden 2006). Quadrupling CO_2 evokes a different response, with the AMIP configurations showing an increase in column-integrated water vapor associated with the slight warming of the continents. The aquaplanets experience no surface warming, and so have no significant change in column water vapor. The two models using a narrower AQUA SST distribution (FGOALS-g2 and MIROC5) are readily identified by their relatively dry tropical atmosphere. The intensity of the hydrologic cycle is shown in Fig. 7 by the ratio of tropical average precipitation to column water vapor, providing an inverse time scale that can be thought of as the average time water resides in the tropical

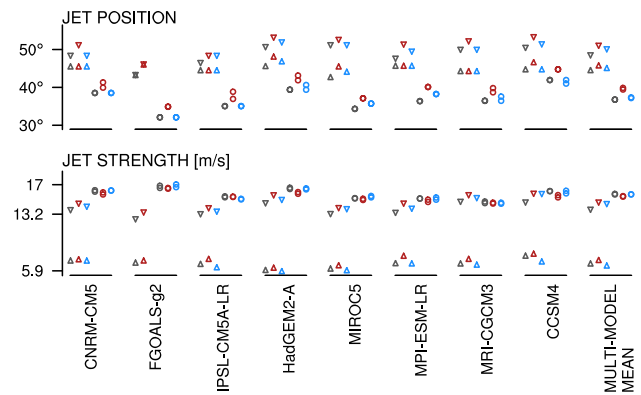


Fig. 6 Eddy-driven jet position (*top*) and strength (*bottom*). Symbols and colors as in Fig. 5. The jet is defined here as the maximum zonal mean zonal wind averaged over the 850 and 700 hPa levels, as in Barnes and Polvani (2013)

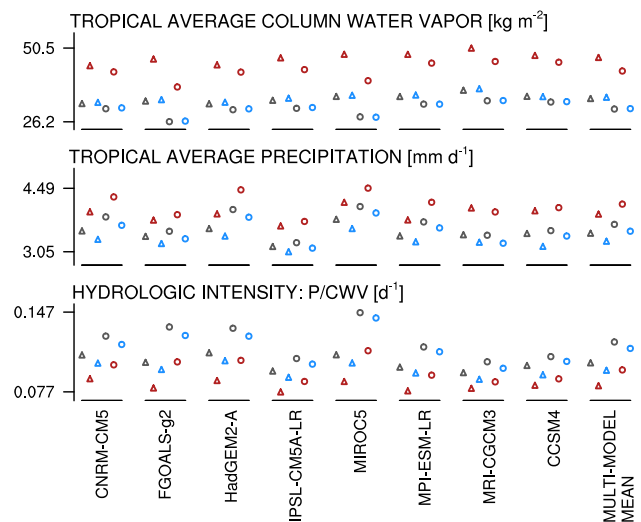


Fig. 7 Diagnostics of tropical hydrologic cycle: *top* vertically integrated water vapor (kg m^{-2}), *middle* precipitation rate (mm d^{-1}), and *bottom* hydrologic intensity, defined as the ratio of precipitation to column water vapor (d^{-1})

atmosphere before being rained out (or being exported to higher latitudes). This hydrologic intensity is greater in AQUA than AMIP configurations, but the responses are similar and the AQUA results capture the spread of the AMIP responses. In all cases the hydrologic intensity is diminished with increased SST or CO_2 , with more weakening in the warming experiments.

This brief survey shows that the responses in the tropical distributions of mass, momentum, and water are comparable in the AMIP and AQUA experiments. The robust responses of the tropical circulation and hydrologic cycle are also comparable to coupled model results (e.g., Held

and Soden 2006; Bony et al. 2013a). There are some indications that the similarities extend beyond the tropics, but the differences in the circulation make the comparison less clear. Keeping such similarities in the large-scale circulation in mind, we next turn to cloud changes.

4 CRE response

Figure 8 shows the dynamical regimes decomposition for all the models and the ensemble mean. There is substantial spread among the models, somewhat more so for convective regimes ($\omega_{500} < 0$). For most models, and the ensemble mean, the CRE increases moderately with ω_{500} , implying that the dynamic term must be small. The intermodel spread in CRE for a given ω_{500} , however, is as large as the variation of CRE across ω_{500} for a given model. The spread in the Δ CRE is similarly large. On average, Δ CRE depends more on dynamical regime in the AMIP experiment (decreasing in magnitude with increasing ω_{500}) than in the AQUA experiment. The thermodynamic and dynamic contributions account for the area covered by each ω_{500} interval and show that the weak vertical motion regimes contain much of the signal, and likewise the spread, by virtue of their prevalence (Fig. 4, middle panels). The AQUA experiments show a similar magnitude of spread in \mathcal{T} , also predominantly in regions of weak subsidence, but the magnitude of this term is somewhat less than in the AMIP experiments. In AMIP and AQUA experiments the dynamical contribution, \mathcal{D} , is confined to a narrow range near the peak of the subsidence distribution where CRE is relatively flat, so these terms have relatively little net effect.

An indication of the difficulty in distinguishing cloud types using only ω_{500} is provided by comparing the ensemble mean CRE with the ω_{500} –LTS joint distribution (Fig. 4). The AMIP configuration shows that CRE (on average) is more sensitive to LTS than ω_{500} variation, indicating a mix of cloud types for a given subsidence regime. On the other hand, the AQUA configuration shows a smaller range of CRE with weaker variation in both dimensions, but in subsidence regimes the CRE remains more strongly dependent on LTS. This picture of the mean CRE variations supports using LTS within subsidence regimes to tease apart the radiative distinctions among boundary layer clouds. The distribution of LTS within subsidence regimes is shown in the bottom panels of Fig. 4. As in the ω_{500} –LTS joint distribution, the AMIP and AQUA configurations exhibit different behavior, with the AMIP configurations being more positively skewed with a tail toward large LTS and AQUA having a more symmetric and narrower distribution. The CRE decreases substantially (i.e., becomes more negative) with increasing LTS in the

AMIP configuration, while the mean AQUA CRE shows a slight weakening (i.e., CRE increases) with LTS; individual models vary in this dependence. This difference suggests that the AQUA simulations do not maintain strong inversions necessary for subtropical stratocumulus decks that form over cool eastern boundary currents of the major ocean basins where the LTS commonly reaches values larger than 18 K (Medeiros et al. 2008; Medeiros and Stevens 2011). In the SST+4K experiments, both configurations show a shift to higher LTS, commensurate with the surface warming.

The upper-left panel of Fig. 9 shows the tropically averaged CRE in the warming experiments. The figure directly compares CRE between AMIP and AQUA for each model (colors), in both the control simulation (filled circle) and the SST+4K climate (unfilled circle; colors as in Figs. 1, 3). The magnitude of Δ CRE is shown by the length of the lines connecting circles, and the slope of the line qualitatively shows whether the AMIP and AQUA configurations have Δ CRE in the same direction (positive slope) or opposed responses (negative slope). Three models show a negative slope, indicating the AQUA Δ CRE has the opposite sign of the AMIP Δ CRE. These models (FGOALS-g2, MPI-ESM-LR and MRI-CGCM3) are further distinguished from the others by plotting them with transparent markers. The inconsistency between the AMIP and AQUA Δ CRE is also evident in Fig. 3. For the other five models, the sign of Δ CRE is consistent between AMIP and AQUA SST+4K experiments. The models are not stratified by mean CRE or by differences between the AQUA and AMIP configurations, so biases in these parameters of the control climate do not appear to be connected to the spread in climate sensitivity, but the tendency for the models to lie along the diagonal suggests that models with a relatively large CRE in the AMIP simulation also have a large CRE in the AQUA configuration.

The remaining panels of Fig. 9 extend this view of the cloud response by focusing on approximate quintiles of ω_{500} . Each panel captures roughly 20 % of the tropics based on the AMIP ensemble mean ω_{500} distribution in Fig. 4. The top row (right two panels) are convective regimes that have net ascent, and the bottom row shows subsidence regimes. The axes remain the same across panels, but are marked to show the ranges in each dimension. Among the models in which the AMIP and AQUA Δ CRE are consistent, the consistency is generally maintained across regimes. Except for MIROC5, the models tend toward similar CRE values with decreasing upward motion, and cluster in the upper right of the diagram for all three subsidence regimes. For some models the consistency between AMIP and AQUA breaks down in particular regimes, usually the strong convection or strong subsidence regimes. The models with inconsistent AMIP

Fig. 8 Dynamical regimes analysis showing CRE in intervals of ω_{500} for the multimodel mean (black line) and individual models (gray dots). Top row shows the mean CRE, second row is the change in CRE in each ω_{500} interval, the third row is the thermodynamic contribution to the change in CRE, and the bottom row is the dynamic contribution to the change in CRE. Axes in left and right columns are the same in each row; tick marks show the extrema and (unweighted) average among the models

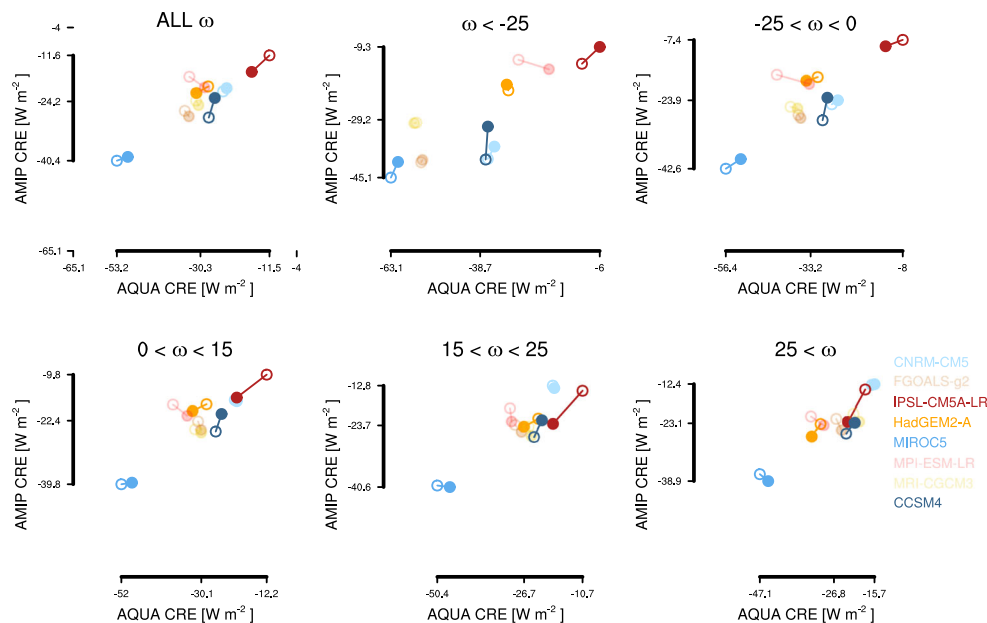
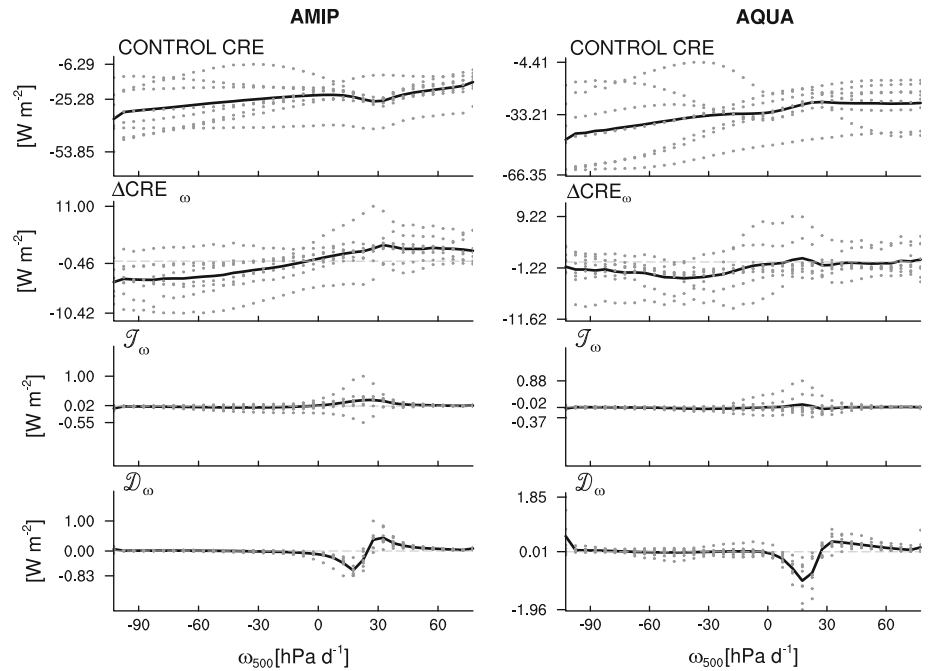


Fig. 9 Net CRE (W m^{-2}) sorted by ω_{500} (hPa d^{-1}). Upper left shows tropical average, and the other panels show ranges of ω_{500} each covering approximately 20 % of the tropics in the AMIP control simulations. Solid circle shows the control simulation values, open

circle shows the SST+4K values. Axes are identical in each panel, but are marked to show the range and mean in each panel in each dimension. The upper left panel labels the full range for reference

and AQUA ΔCRE also show less consistency across regimes; no single ω_{500} regime appears to dominate the inconsistent responses.

Whether a model's AQUA ΔCRE agrees with its AMIP counterpart appears to depend on the structure of the tropical circulation. In this ensemble of models, aquaplanets with a twin ITCZ structure have a ΔCRE that is

consistent with their AMIP counterparts, but those with a single ITCZ on the equator differ from their corresponding AMIP experiment. Those models have positive AMIP ΔCRE and negative AQUA ΔCRE . Figure 10 shows this division in the zonal mean precipitation in the AQUA control simulations and the change in zonal mean precipitation with SST+4K. The only AQUA SST+4K

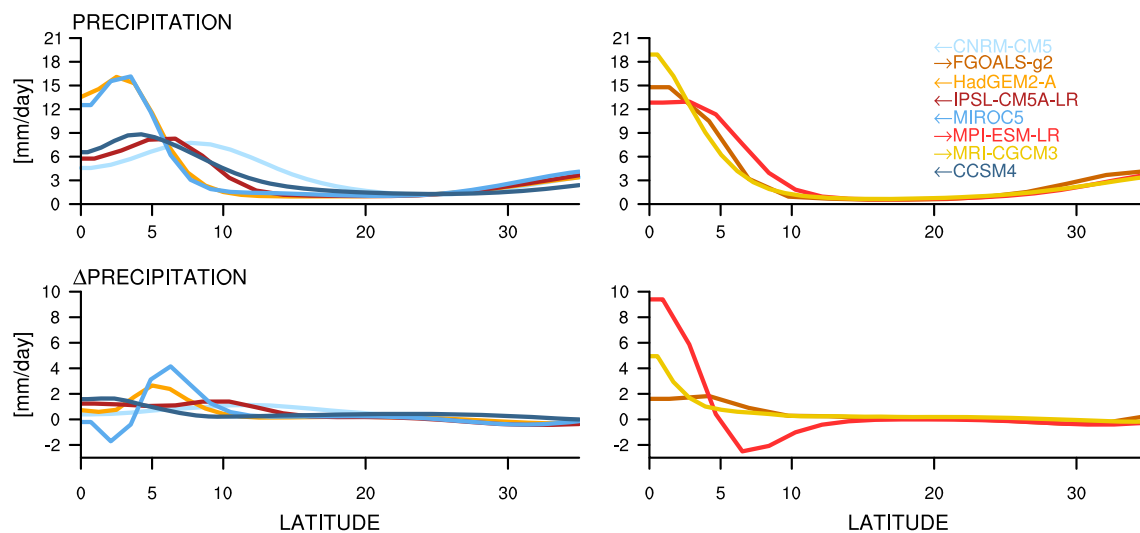


Fig. 10 Zonal mean precipitation for the AQUA control simulations in *top panels*, and the change with SST+4K on the *bottom*. *Left panels* shows those models where the AQUA Δ CRE is consistent (*in sign*) with the corresponding AMIP experiment. *Right panels* show

models with an inconsistent Δ CRE between the configurations. *Colors* are as in previous figures; *arrows* in the legend point toward the column in which each model appears

experiment with a single ITCZ and positive Δ CRE is from NICAM-09. That model does not parameterize deep convection, and it develops a single ITCZ on the equator that produces more precipitation than any of the conventional GCMs and has a positive tropical Δ CRE with relatively high sensitivity (Table 1).

To test the connection between ITCZ structure and cloud response, we conducted additional experiments with the MPI-ESM-LR and CCSM4. A SST pattern that is much flatter across the tropics was applied to the MPI-ESM-LR, and resulted in a twin ITCZ structure and a positive tropical Δ CRE in the SST+4K experiment, which matches the AMIP Δ CRE. A complementary experiment with the CCSM4 used a strongly peaked SST pattern that produced a single ITCZ, but that experiment produced a negative Δ CRE like the other CCSM4 experiments. The Δ CRE was stronger than for the standard AQUA experiment, possibly suggesting that the presence of a single ITCZ produces a smaller (possibly more negative) Δ CRE than in twin ITCZ configurations. Without further experimentation, however, the intriguing connection between ITCZ structure and cloud response should not be considered robust: other factors are likely to be relevant. One factor not accounted for in fixed SST experiments like those used here is the possibility that extratropical climate response has an influence on tropical feedbacks and the structure of the ITCZ (e.g., Kang et al. 2009), raising the possibility that an interactive lower boundary might produce a different relationship between the ITCZ and cloud response.

From the dynamical regimes analysis along with the results in Fig. 3, the well-known result emerges that

climate sensitivity varies among climate models, mostly due to differing responses of low-latitude clouds under subsidence (cf. Bony and Dufresne 2005; Vial et al. 2013). The dynamical regimes analysis connects the spread in cloud response to regimes with weak vertical motion. The spread among the models arises more from the spread in the thermodynamic contribution, as cloud properties in the weak vertical motion regimes change differently across models. As shown by Fig. 4, the vertical motion alone does not distinguish among boundary layer cloud types. To separate these cloud types, LTS can be used; the distribution of LTS differs between the AMIP and AQUA configurations due to stratocumulus regions in the AMIP configuration characterized by large LTS.

4.1 The inconsistent models

Of the eight independent models with adequate output for this analysis (Table 1), five have a consistent tropical cloud response in the AMIP and AQUA configurations, but three have inconsistent responses. There appears to be a connection to ITCZ structure, but this connection does not fully explain the inconsistencies. As mentioned, the discrepancy in Δ CRE appears mainly in the weak vertical velocity regimes, and mostly due to differences with the thermodynamic contribution of the response, i.e., changes in the cloud properties within ω_{500} -regimes. In this section, we take a closer look at the three inconsistent models to determine if particular cloud types or features can account for the differing response to warming in the AMIP and AQUA settings.

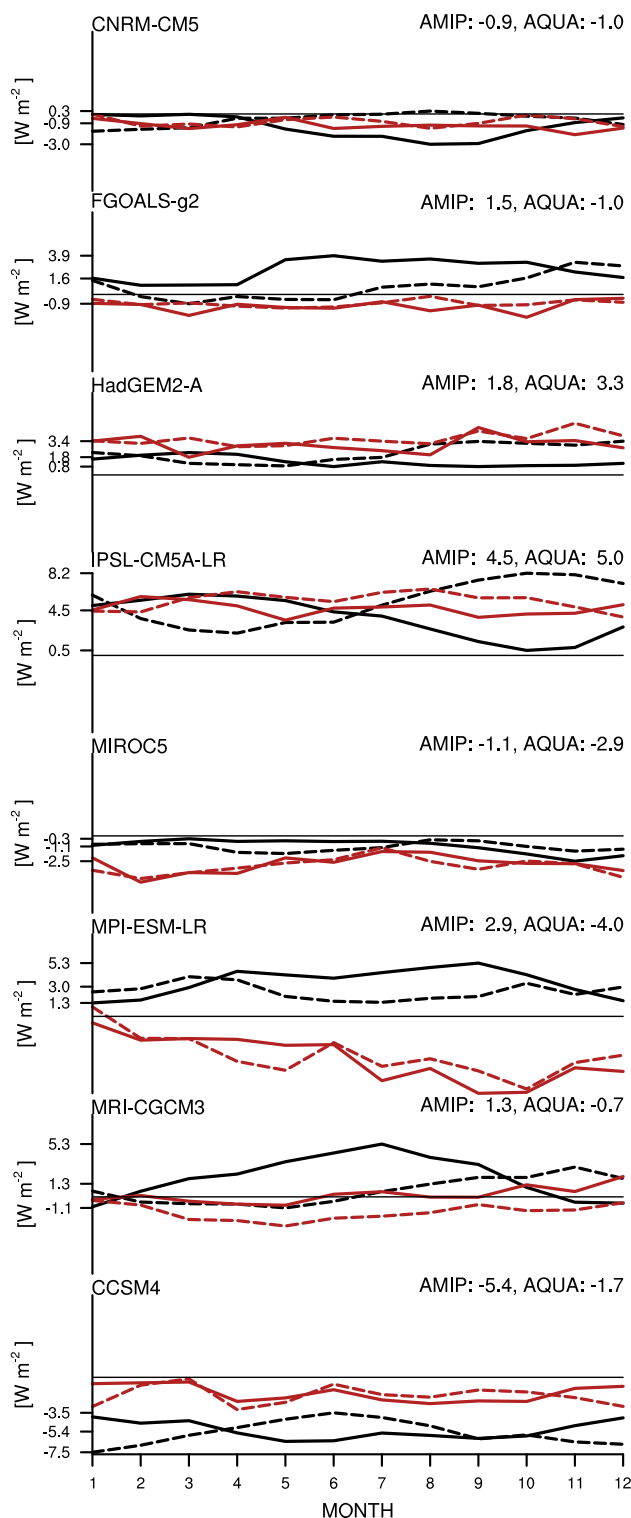


Fig. 11 Change in CRE in each calendar month for each model. Black lines show the AMIP configuration and red lines the AQUA configuration. Solid lines show the northern hemisphere, and dashed lines show the southern hemisphere. Tropical averages are given at upper right of each panel. Land is neglected for the AMIP configurations

Seasonal or hemispherically asymmetric responses may occur in the AMIP experiments that are absent from the AQUA configuration. Figure 11 shows the annual cycle of ΔCRE separately for the northern and southern hemispheres in the SST+4K experiments. No systematic effects appear to explain differences between the AQUA and AMIP results. The AQUA experiments, by construction, lack seasons and hemispheric asymmetry, so variations in the AQUA annual cycle express internal variability. Spectral analysis (not shown) confirms that none of the AQUA simulations has a statistically significant annual cycle, and only MRI-CGCM3 AQUA exhibits any hemispheric asymmetry. The AMIP configurations have significant seasonal variations, but without consistent structure across models (Table 3). Most models have similar responses in each hemisphere, but FGOALS-g2 and MRI-CGCM3 show substantially stronger positive CRE changes in the northern hemisphere, perhaps signaling a role for zonal asymmetries in the AMIP ΔCRE .

Figure 12 shows the geographic distribution of CRE (left) and ΔCRE (right) for the three models with inconsistent ΔCRE between the AMIP and AQUA experiments (the other models are shown in Online Resource 1). In the left panels, contour lines show the LTS distribution overlaid on the CRE (color shading). Here, as in previous studies (Klein and Hartmann 1993), regions of large LTS are associated with the quasi-permanent subtropical stratocumulus decks which distinguishes them from the broader trades that are dominated by shallow, trade-wind cumulus. Also as previously shown (Medeiros and Stevens 2011), the AQUA configurations do not support stationary regions of stratocumulus; LTS rarely exceeds 15 K in the AQUA configuration (cf. Fig. 4).

Stratocumulus regions in FGOALS-g2 and MRI-CGCM3 carry a disproportionate amount of the tropical ΔCRE signal. For FGOALS-g2, about half of the AMIP ΔCRE is contained in the 5 % of points with the largest LTS, which are concentrated in these stratocumulus decks. For MRI-CGCM3 (Yukimoto et al. 2012) this link is even more pronounced, with about 60 % of the positive ΔCRE accounted for by points in the top 5 % of LTS. In the other models, the fraction is typically around 10 %; the next largest value is for HadGEM2-A with about 25 % of its ΔCRE in the most stable regions. In the warming scenario the stratocumulus decks of FGOALS-g2 and MRI-CGCM3 are greatly diminished (Fig. 12). This is also evident in Figs. 13 and 14 which present the vertical structure of clouds in the subsidence regions divided by large and moderate LTS. At moderate values of LTS (left panels of figures), the AMIP and AQUA configurations show similar cloud structures (though the two models greatly differ from each other). In the high-stability

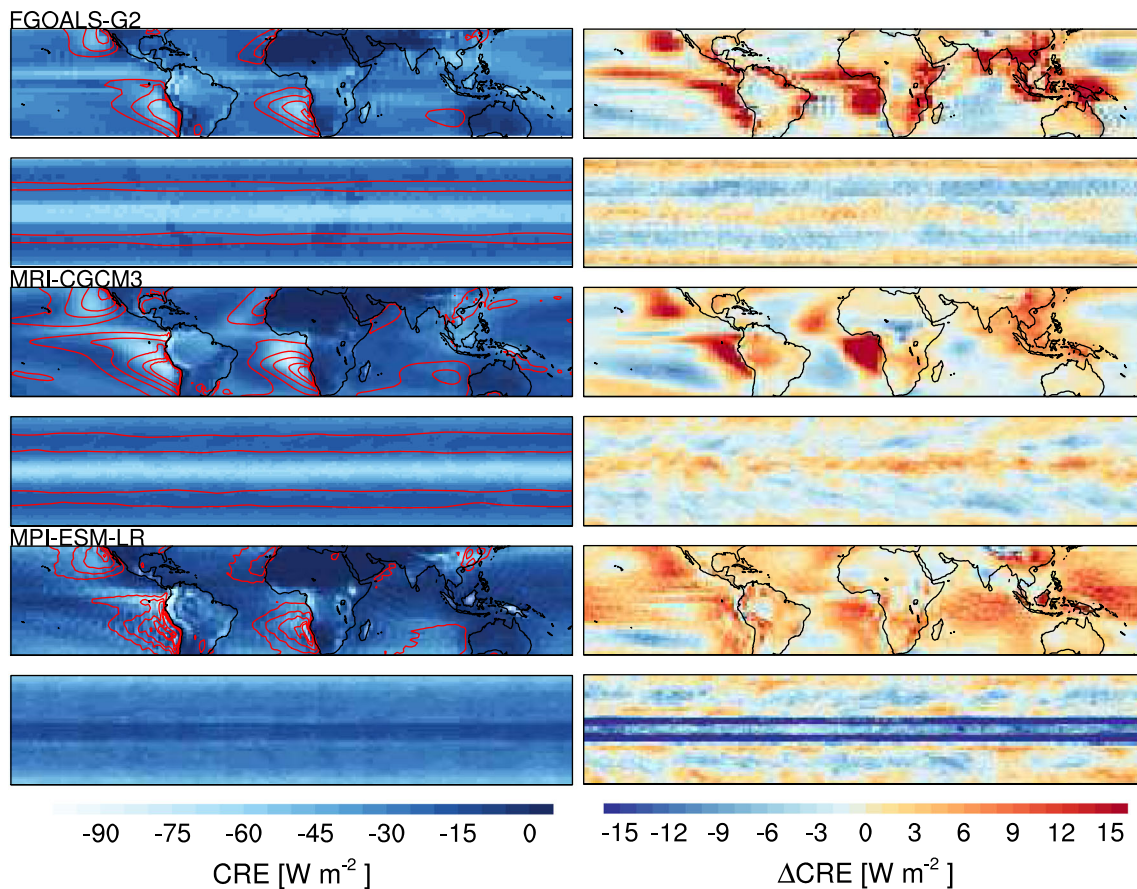


Fig. 12 Mean CRE in the three inconsistent models in their AMIP and aquaplanet simulations (*left panels*) and Δ CRE from the warming experiments in the *right panels*. In the left panels LTS is contoured in

red, from 14.5 to 21.5 K by 2 K. The MPI-ESM-LR AQUA has a maximum mean LTS in the tropics of 14.1 K, so no contours are displayed

Table 3 Tropical ocean Δ CRE (W m^{-2}) in each hemisphere of the AMIP configurations

Model	NH	SH
CCSM4	−5.26	−5.54
CNRM-CM5	−1.28	−0.57
FGOALS-g2	2.40	0.77
HadGEM2-A	1.34	2.19
IPSL-CM5A-LR	3.69	5.27
MIROC5	−1.01	−1.09
MPI-ESM-LR	3.43	2.48
MRI-CGCM3	1.97	0.63

Land has been removed

regime, the AMIP configurations show lower, cloudier cloud layers indicative of stratocumulus, but this regime is not represented in the AQUA configurations. In both models, this low-level cloud layer in regions of large LTS becomes less cloudy with warming, and cloud amount increases at higher levels indicating a transition toward more cumulus-like conditions. Because this large LTS regime is not

represented in the AQUA experiment, such a response is also absent. The AQUA SST+4K simulation has some data in the high-stability category; this occurs because the LTS distribution shifts by about 2 K with the warming, a feature common to all the models (Fig. 4). Most of the disparity between the AMIP and AQUA experiments for FGOALS-g2 and MRI-CGCM3 can thus be attributed to the strong positive Δ CRE in the stratocumulus regions—which the AQUA simulations do not represent—as the rest of the trade-wind regions show small CRE changes. Though they have similar stratocumulus responses, these models determine cloud fraction in different ways: FGOALS-g2 diagnoses cloud fraction based on relative humidity and LTS while MRI-CGCM3 predicts cloud fraction following Tiedtke (1993). This finding is counter to the conclusion in Medeiros et al. (2008) that the statistical weight of the trade-wind cumulus regimes overwhelms the tropical CRE response; these models appear to have stratocumulus that are more vulnerable to surface warming than the models in that study or the other models in this study.

Figure 12 suggests that MPI-ESM-LR is less dominated by zonal asymmetries, and Fig. 11 shows that seasonal

Fig. 13 Cloud amount profiles for tropical subsidence regimes in FGOALS-g2. *Left* relatively unstable locations ($LTS < 18\text{ K}$), and *right* stable locations ($18\text{ K} < LTS$). *Solid lines* show the control simulations, *lighter dashed lines* show the SST+4K simulations

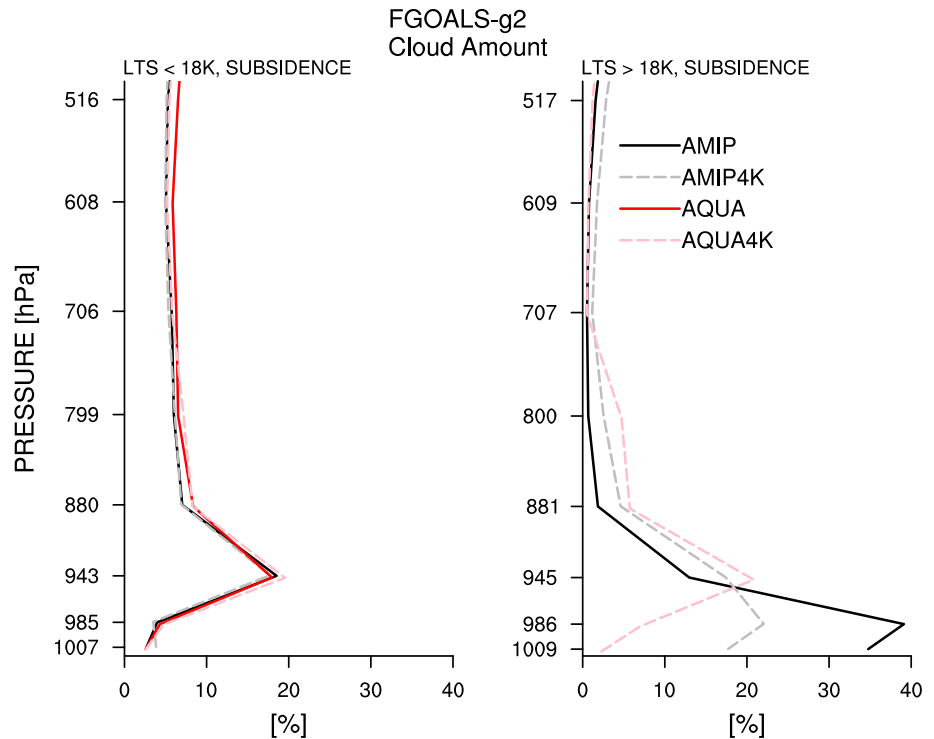
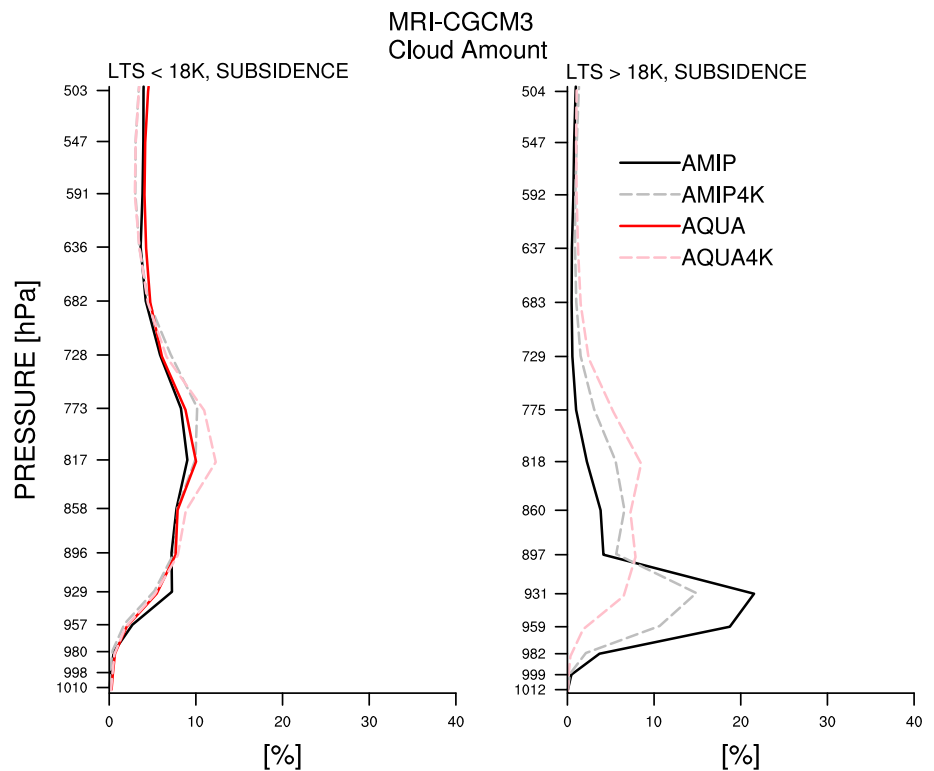


Fig. 14 Cloud amount profiles for tropical subsidence regimes in MRI-CGCM3, as in Fig. 13



patterns are not a leading cause of the disagreement between the AMIP and AQUA cloud responses. The largest values of LTS carry little of the ΔCRE in either configuration. Instead, the AMIP configuration shows widespread

positive ΔCRE , and the AQUA shows strong negative ΔCRE in the deep tropics and weaker negative ΔCRE in the subtropics. Two latitudinal bands of negative ΔCRE occur on either side of the equator, where the ITCZ

Fig. 15 Difference in zonal mean vertical velocity (ω , hPa d⁻¹, shading) and cloud amount (percent, lines) for SST+4K experiments with the MPI-ESM-LR AMIP (left) and AQUA (right) configurations. Blue contour lines show an increase in cloud amount, gray shows the zero contour, and dashed red shows decreases in cloud amount. Red shading shows anomalous descent while blue shows anomalous ascent. Gray dots at 50 hPa denote latitudes where $\Delta\text{CRE} < -8\text{Wm}^{-2}$

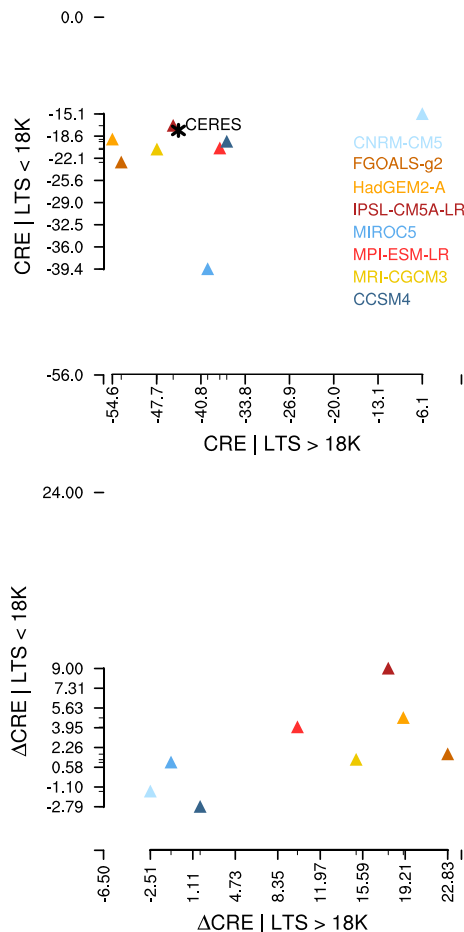
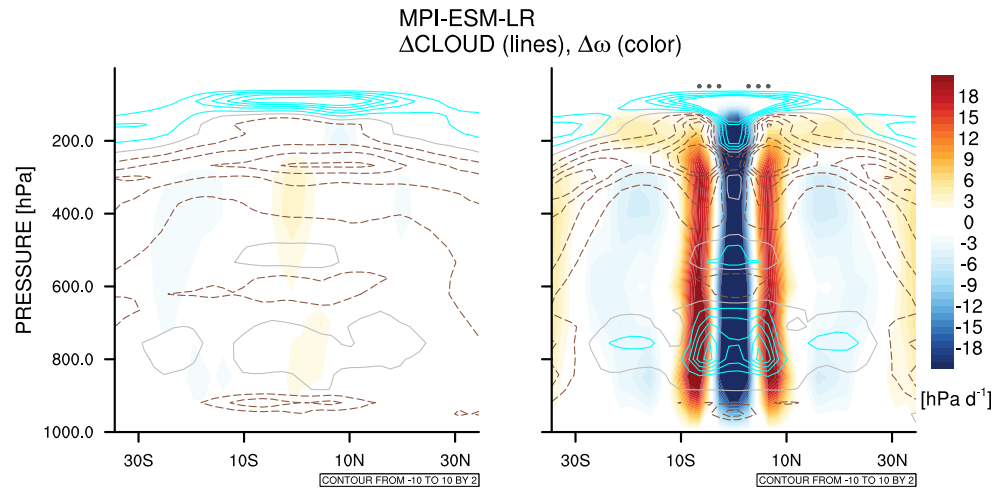


Fig. 16 Top tropical mean CRE (W m^{-2}) conditioned on subsidence and LTS $> 18\text{K}$ (abscissa) or $< 18\text{K}$ (ordinate) for each AMIP control simulation. A satellite estimate is shown in black; it is CERES EBAF (v.2.6r) monthly data from March 2000 through December 2011, and ω_{500} and LTS were derived for corresponding time from ERA-Interim. Bottom The SST+4K ΔCRE similarly sampled. Colors as in previous figures; in each panel the range of the horizontal and vertical axes are the same

narrows from the control to SST+4K simulation and there is anomalous subsidence. The MPI-ESM-LR AQUA SST+4K experiment is the only one that shows a strengthening Hadley circulation (Table 2). Associated with the slight strengthening, the dynamic contribution to the ΔCRE is particularly strong in the AQUA experiment (Fig. 8). Figure 15 summarizes this change, and shows that the bands of negative ΔCRE are due to increased cloud cover at the margins of the tropical convergence zone.

Inconsistent cloud responses between the AMIP and AQUA configurations arise in this ensemble of models for two reasons. On the one hand, the FGOALS-g2 and MRI-CGCM3 have zonally asymmetric features in their AMIP cloud responses that carry much of the ΔCRE signal, but are not represented in the AQUA configuration. On the other hand, the reorganization of the ITCZ in the MPI-ESM-LR AQUA experiment is fundamentally different than that of the AMIP configuration. While these three models demonstrate the largest differences between the AMIP and AQUA configurations, other models may share some of these features but with a smaller influence on the tropical-average climate change. The results raise important questions about the mechanisms of cloud feedback in climate models. For example, what mechanisms, particularly for FGOALS-g2 and MRI-CGCM3, make stratocumulus decks so susceptible to dissipation with increased SST while the broader trades actually become cloudier?

Because the stratocumulus response is important in some models, it is interesting to compare changes in stratocumulus regions to trade-wind cumulus regions across models. Figure 16 divides the tropical subsidence regimes by stability (as in Figs. 13 and 14), comparing CRE (top panel) and ΔCRE (bottom panel) in the lower versus higher stability regions for the AMIP SST+4K experiments. Mean CRE strongly differs between the stability-separated regions: the clustering of points in the upper left show the

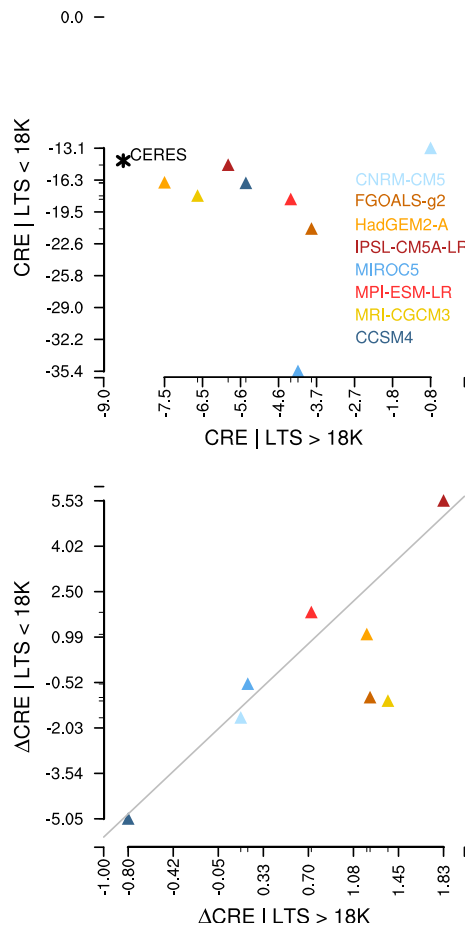


Fig. 17 As in Fig. 16, but each regime's contribution to the tropical average CRE (conditioned on subsidence). The contribution is determined by averaging relative to the area of all subsidence regimes over the tropical oceans. To calculate the contribution to the change in CRE, the same method is applied, but using the same locations for the warming case as the control case. This is applied on a month-by-month basis and then averaged, which mixes regimes in the warming case, but it is hoped in a random way. The *gray line* shows the linear regression neglecting the two outliers (see text). *Colors* as in previous figures; in each panel the *vertical axis* range is four times that of the *horizontal* range

different radiative effects of stratocumulus decks and trade-wind cumulus regions and confirms that this LTS-based division appropriately separates these cloud types. An estimate of the observed CRE using CERES CRE and ERA-Interim LTS and ω_{500} is also shown. Two of the low-sensitivity models show substantial biases compared to the CERES estimate: CNRM-CM5 (Voldoire et al. 2012) has stratocumulus regions with a net CRE that is much too weak, and MIROC5 (Watanabe et al. 2010) has trade-wind regions with an overly strong negative CRE. The lower panel shows Δ CRE, and shows the separation between the higher and lower sensitivity models. Both FGOALS-g2 and MRI-CGCM3 have small positive Δ CRE in the trade-wind cumulus regions (low LTS) and much larger values for the stratocumulus regions (large LTS). The other high

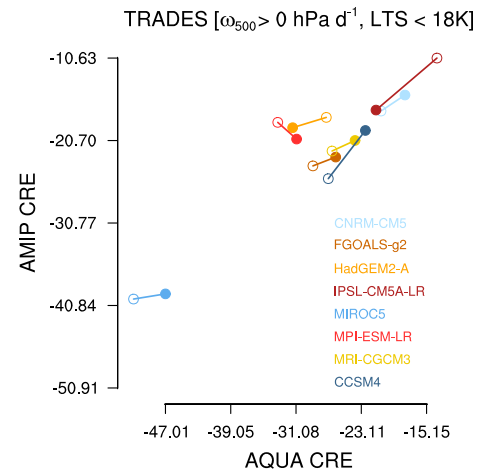


Fig. 18 CRE (W m^{-2}) averaged over the trade-wind regions, displayed as in Fig. 9

sensitivity models show stronger positive Δ CRE in the trade-wind regions. This separation shows that biases in the mean CRE do not necessarily translate to Δ CRE, but it is difficult to compare Δ CRE between regimes because of differences in areal coverage. A better comparison is shown by Fig. 17, in which averages are again calculated for tropical subsidence regimes but here using the relative area of the trade-wind or stratocumulus regions. The larger values for the lower-stability regions in the upper panel reflect the much larger area covered by trade-wind cumulus conditions compared to the relatively rare stratocumulus decks. The observation-based point, however, shows a stronger mean CRE for stratocumulus points than any of the models and is on the weaker CRE side for the trade-wind cumulus points; this reaffirms the finding of Medeiros and Stevens (2011) that climate models struggle to maintain the large-scale environment that fosters quasi-permanent subtropical stratocumulus and often predict shallow cumulus clouds that are too reflective (Nam et al. 2012). The lower panel of Fig. 17 similarly shows Δ CRE using the control simulations to sample the SST+4K simulations, i.e., points that are in the stratocumulus sample in the control simulation are considered in the stratocumulus sample in the warming simulation. The figure shows the regression line excluding the outliers FGOALS-g2 and MRI-CGCM3. The slope of the regression is 3.78 and is significant ($p = 0.0015$), so most models with a strong CRE response have it predominantly from trade-wind cumulus regions. Only the CCSM4 (Gent et al. 2011) has a negative Δ CRE in the stratocumulus regions, but excluding it only reduces the regression slope to 3.65. The two models with strong zonal asymmetries in Δ CRE (FGOALS-g2 and MRI-CGCM3) show stronger positive Δ CRE in the stratocumulus regions than their negative Δ CRE in the trade-wind cumulus regions. This simple division of contributions suggests that

the prevalence of trade-wind cumulus conditions typically determines the tropical-average cloud response, but for a minority of models the stratocumulus regions have an out-sized effect on the tropical average.

Knowing that the dissipation of subtropical stratocumulus decks leads to AMIP–AQUA inconsistency in FGOALS-g2 and MRI-CGCM3 provokes a reexamination of the role of the broader trades. As shown above, the subsidence regimes with relatively low static stability account for most of the CRE change in most models. Figure 18 expands on this finding by focusing on the trade-wind regions of the control simulations. The figure shows that sampling those regions in the SST+4K simulations shows improved consistency between the AMIP and AQUA Δ CRE; seven of the eight models agree on the sign, compared to five in Figs. 3 and 9. The MPI-ESM-LR remains as the sole outlier because the AQUA Δ CRE is heavily influenced by the transition from upwelling to subsidence along the edges of the convection zone. The consistency between configurations in Fig. 18 is sensitive to the choice to sample the locations from the control simulations; this is because the AMIP configurations show more diversity in the structure of low-level clouds (such as hybrid cloud types along the stratocumulus-to-cumulus transitions).

5 Adjusted forcing

In this section, we compare the AMIP and AQUA tropospheric adjustment to quadrupling atmospheric CO_2 . With prescribed SST and sea-ice, $4 \times \text{CO}_2$ experiments are designed to isolate changes in the climate due only to the direct radiative impact of CO_2 with no surface-temperature feedbacks. This adjustment can be considered as a climate forcing (i.e., not a feedback, Andrews and Forster 2008); it is also called “effective radiative forcing” (e.g., IPCC 2013) or simply radiative forcing. As noted above, the climate sensitivity parameter is ill-defined in these experiments because the surface temperature does not change. In actuality, however, the land surface component is active in the AMIP configuration, and the land warms in response to the altered atmospheric composition. This warming is small, but can evoke large-scale circulations which may impact estimates of the adjusted forcing (Wyant et al. 2012; Bony et al. 2013a). The AQUA experiment offers an idealized view of the adjusted forcing that is free from any surface feedbacks (and thus consistent with the concept of adjusted troposphere and stratosphere forcing of Shine et al. 2003). Differences between the AMIP and AQUA $4 \times \text{CO}_2$ experiments indicate the role of land surface effects in previous descriptions of the adjusted forcing (see also, Bony et al. 2013a).

The adjusted forcing is shown in the top panels of Fig. 19, comparing the AMIP and AQUA values for each

model. Most models (except IPSL-CM5A-LR and CCSM4) have greater global forcing values in the AQUA configuration, with similar results for the tropics. This suggests that warming the continents modestly reduces the adjusted forcing in the AMIP configurations.

As a response to $4 \times \text{CO}_2$, infrared cooling reduces (and the troposphere warms), the Hadley circulation expands and weakens slightly (Fig. 5), the eddy-driven jet migrates slightly poleward (Fig. 6), tropical precipitation is inhibited, and the hydrologic cycle intensifies slightly (Figs. 7 and 19). Though subsidence generally weakens, the warming is greatest in the lower troposphere, increasing LTS (Fig. 19). This enhanced stability is greater in the AMIP experiment as convection shifts onto the continents with compensating subsidence preferentially over oceans. Stronger stability leads to weaker cloud-top entrainment and shallower boundary layer depth (Wyant et al. 2012) along with reduced low-level relative humidity and decreased latent heat flux (Kamae and Watanabe 2012). As a result of this chain of processes, all models considered here have decreased cloud cover, smaller condensate water path, weaker shortwave and longwave CRE, and weaker clear-sky longwave radiative forcing (not shown). The net effect of CRE is more varied, shown in the bottom panels of Fig. 19. The varying sign of the net CRE response among the models likely arises from cloud masking effects rather than redistributions of clouds in the vertical (Kamae and Watanabe 2012). Previous studies have estimated cloud masking effects in such experiments to be around 1 Wm^{-2} , which would seem to account for the differing signs in Δ CRE, though confirmation requires additional, unavailable model output. The spread among models, like in the warming experiments, is due to differences in the shortwave CRE response in subsidence regimes. Kamae and Watanabe (2012) attribute some of the model spread to differences in the specific humidity structure at low levels.

The direct response to $4 \times \text{CO}_2$ is smaller than the response to surface warming (Table 1), and is not always consistent with the warming experiments. This suggests that, consistent with the findings of Vial et al. (2013) and Zelinka et al. (2013), a failure to account for rapid adjustments likely has little influence on the inter-model spread of estimates of the feedback strength.

6 Summary

This analysis shows that idealized, fixed-SST climate change experiments are useful for understanding the equilibrium response of more realistic model configurations. This finding is surprising given the importance of ocean processes and SST feedbacks in the climate system

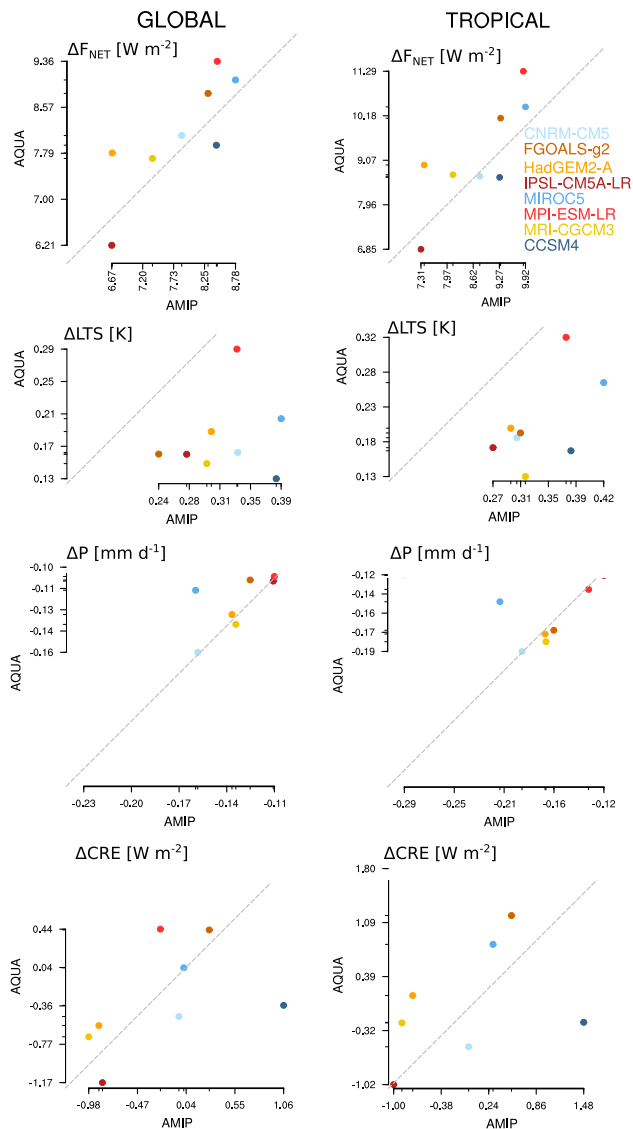


Fig. 19 Global (left) and tropical (right) average responses in the $4 \times \text{CO}_2$ experiments, *top-to-bottom* adjusted forcing (ΔF_{NET} , W m^{-2}), lower-tropospheric stability (K), total precipitation (mm d^{-1}), and CRE (W m^{-2}). Values include land grid points except for LTS, which includes ocean locations only

and recent studies that point out the importance of ocean heat uptake in transient climate change experiments (Raper et al. 2002; Winton et al. 2010; Armour et al. 2013; Rose et al. 2014). A number of robust responses to SST warming are found in the AMIP and AQUA settings. Warming induces a widening and weakening of the Hadley cells, and a poleward migration of the eddy-driven jet. Column water vapor and precipitation increase with warming in both configurations, balancing the weakened Hadley circulation. Cloud responses to warming vary widely among the models, controlling the spread in climate sensitivity. This result shows that much of the

spread in estimates of climate sensitivity derives from the simplest expression of cloud feedbacks (i.e., the response to uniform warming).

Five of the eight models have a consistent cloud response to SST warming between configurations. Three models' AQUA experiments have smaller climate sensitivity than the corresponding AMIP experiment, each having negative ΔCRE in AQUA versus positive in AMIP. In the AMIP experiment, two of these models (MRI-CGCM3 and FGOALS-g2) are dominated by positive ΔCRE focused in stratocumulus regions. The AQUA configuration does not support stratocumulus decks, so does not capture the diminishing cloud cover of the AMIP experiments in those regions. The MPI-ESM-LR AQUA response is fundamentally different as its ITCZ narrows, converting area from deep convection regimes to weak vertical motion regimes dominated by boundary layer clouds with a strong shortwave CRE.

All three models with inconsistent ΔCRE between configurations have a single ITCZ on the equator in the AQUA configuration, while all the other models have a twin-ITCZ structure. Sensitivity experiments with MPI-ESM-LR show that splitting the ITCZ can change the ΔCRE from negative to positive. The reverse effect was not found with CCSM4, however, hinting that AQUA configurations with a single ITCZ may tend toward negative ΔCRE . The NICAM-09, which avoids cumulus parameterization, is a counterexample, but longer simulations are needed to determine the robustness of that model's climate response.

Separating the stratocumulus and trade-wind cumulus regimes (Figs. 16, 17) indicates that the tropical average ΔCRE is influenced by the trade-wind cumulus regime ($\omega_{500} > 0 \text{ hPa day}^{-1}$, $\text{LTS} < 18\text{K}$) nearly four times more than the stratocumulus regimes ($\omega_{500} > 0 \text{ hPa day}^{-1}$, $\text{LTS} > 18\text{K}$) except for the two models where the stratocumulus response is pronounced. The AQUA SST warming experiments show striking similarity in the structure and response of shallow trade-wind cumulus to the AMIP warming experiments (Fig. 18). As these clouds carry much of the cloud response signal in these models, aquaplanets provide an ideal setting to understand it.

When atmospheric CO_2 is quadrupled and SST held fixed, the models produce robust responses in AMIP and AQUA configurations. Circulation changes are smaller than for SST warming, but the Hadley circulation weakens when infrared cooling decreases and stability increases. Tropical precipitation is inhibited by the change in stability and vertical motion. In the AMIP configurations, the interactive land surface shifts precipitation from oceans to continents and induces continental-scale anomalous circulations. Comparing to the AQUA experiments, therefore,

exposes land-surface effects, which appear to slightly moderate the adjusted forcing. The cloud response to quadrupling CO₂ is smaller than to surface warming. The variation in sign of the longwave and shortwave components of Δ CRE are robust, but the sign of Δ CRE is not. This is likely due to the $\approx 1 \text{ Wm}^{-2}$ cloud masking effect while the spread among models in Δ CRE is associated with differing shortwave CRE changes mostly in the boundary layer clouds of weak subsidence regimes.

For understanding the processes that control climate change, these idealized climate model configurations prove to be useful tiers in the hierarchy of models. Both AMIP and AQUA experiments show similar, robust responses of the tropical circulation and hydrologic cycle, which are comparable to changes in more complex configurations. The AMIP experiments also show similarity to coupled experiments in estimates of climate sensitivity. The AMIP configuration captures aspects of the fully coupled system while removing the influence of SST biases and feedbacks, and warming experiments in the AMIP setting focus attention on tropical cloud responses in the absence of interaction with the surface. The further idealized AQUA configuration in turn removes the complications of zonal asymmetries, and emphasizes the role of shallow cumulus convection in both forcing and feedback. The present analysis confirms that regions dominated by shallow cumulus are crucial to the overall tropical cloud response to increased CO₂ and warming.

Acknowledgments We acknowledge the World Climate Research Programme's Working Group on Coupled Modelling, which is responsible for CMIP, and we thank the climate modeling groups (Table 1) for producing and making available their model output. For CMIP the U.S. Department of Energy's Program for Climate Model Diagnosis and Intercomparison provides coordinating support and led development of software infrastructure in partnership with the Global Organization for Earth System Science Portals. Data analysis and figure creation were performed with NCL (2012). We thank Benjamin Möbis for performing the sensitivity runs with the MPI-ESM-LR. B. M. acknowledges support from the Regional Climate Modeling Program (RGCM) of the U.S. Department of Energy's, Office of Science (BER), Cooperative Agreement DE-FC02-97ER62402. B. S. and S. B. acknowledge support from EUCLIPSE (FP7-ENV-2009-1 European Project #244067). NCAR is sponsored by the National Science Foundation.

Open Access This article is distributed under the terms of the Creative Commons Attribution License which permits any use, distribution, and reproduction in any medium, provided the original author(s) and the source are credited.

References

- Andrews A, Forster PM (2008) CO₂ forcing induces semi-direct effects with consequences for climate feedback interpretations. *Geophys Res Lett* 35(4):L04802. doi:[10.1029/2007GL032273](https://doi.org/10.1029/2007GL032273)
- Andrews T, Gregory JM, Webb MJ, Taylor KE (2012) Forcing, feedbacks and climate sensitivity in CMIP5 coupled atmosphere–ocean climate models. *Geophys Res Lett* 39(9):L09712. doi:[10.1029/2012GL051607](https://doi.org/10.1029/2012GL051607)
- Armour KC, Bitz CM, Roe GH (2013) Time-varying climate sensitivity from regional feedbacks. *J Clim* 26(13):4518–4534. doi:[10.1175/JCLI-D-12-00544.1](https://doi.org/10.1175/JCLI-D-12-00544.1)
- Barnes EA, Polvani L (2013) Response of the midlatitude jets and of their variability to increased greenhouse gases in the CMIP5 models. *J Clim*. doi:[10.1175/JCLI-D-12-00536.1](https://doi.org/10.1175/JCLI-D-12-00536.1)
- Blackburn M, Williamson DL, Nakajima K, Ohfuchi W, Takahashi YO, Hayashi YY, Nakamura H, Ishiwatari M, McGregor J, Borth H, Wirth V, Frank H, Bechtold P, Wedi NP, Tomita H, Satoh M, Zhao M, Held IM, Suarez MJ, Lee MI, Watanabe M, Kimoto M, Liu Y, Wang Z, Molod A, Rajendran K, Kitoh A, Stratton R (2013) The Aqua-Planet Experiment (APE): CONTROL SST simulation. *J Meteorol Soc Jpn* 91A:17–56. doi:[10.2151/jmsj.2013-A02](https://doi.org/10.2151/jmsj.2013-A02)
- Bony S, Dufresne JL (2005) Marine boundary layer clouds at the heart of tropical cloud feedback uncertainties in climate models. *Geophys Res Lett* 32. doi:[10.1029/2005GL023851](https://doi.org/10.1029/2005GL023851)
- Bony S, Dufresne JL, Treut HL, Morcrette JJ, Senior C (2004) On dynamic and thermodynamic components of cloud changes. *Clim Dyn* 22:71–86
- Bony S, Bellon G, Klocke D, Sherwood S, Fermepin S (2013a) Robust direct effect of carbon dioxide on tropical circulation and regional precipitation. *Nat Geosci* 6(6):447–451. doi:[10.1038/ngeo1799](https://doi.org/10.1038/ngeo1799)
- Bony S, Stevens B, Held I, Mitchell J, Dufresne JL, Emanuel K, Friedlingstein P, Griffies S, Senior C (2013b) Climate Science for Serving Society: research, modeling and prediction priorities. In: Asrar GR, Hurrell JW (eds) Carbon dioxide and climate: perspectives on a scientific assessment. Springer, p 484
- Boucher O, Randall D, Artaxo P, Bretherton C, Feingold G, Forster P, Kerminen VM, Kondo Y, Liao H, Lohmann U, Rasch P, Satheesh SK, Sherwood S, Stevens B, Zhang XY (2013) Climate change 2013: the physical science basis. In: Clouds and Aerosols. Contribution of Working Group I to the 5th assessment report of the intergovernmental panel on climate change, Cambridge University Press, Cambridge, United Kingdom and New York, NY, USA
- Brient F, Bony S (2012) How may low-cloud radiative properties simulated in the current climate influence low-cloud feedbacks under global warming? *Geophys Res Lett* 39(20):L20807. doi:[10.1029/2012GL053265](https://doi.org/10.1029/2012GL053265)
- Brient F, Bony S (2013) Interpretation of the positive low-cloud feedback predicted by a climate model under global warming. *Clim Dyn* 40(9–10):2415–2431. doi:[10.1007/s00382-011-1279-7](https://doi.org/10.1007/s00382-011-1279-7)
- Cess R, Potter GL, Blanchet JP, Boer GJ, Ghan SJ, Kiehl JT, Treut HL, Li ZX, Liang XZ, Mitchell JFB, Morcrette JJ, Randall DA, Riches M, Roeckner E, Schlesse U, Slingo A, Taylor EE, Washington WM, Wetherald RT, Yagai I (1989) Interpretation of cloud-climate feedback as produced by 14 atmospheric general circulation models. *Science* 245:513–516
- Cess RD, Potter GL, Blanchet JP, Boer GJ, Del Genio AD, Déqué M, Dymnikov V, Galin V, Gates WL, Ghan SJ, Kiehl JT, Lacis AA, Le Treut H, Treut BJ, Meleshko VP, Mitchell JFB, Morcrette JJ, Randall DA, Rikus L, Roeckner E, Royer JF, Schlesse U, Sheinin DA, Slingo A, Sokolov AP, Taylor KE, Washington WM, Wetherald RT, Yagai I (1990) Intercomparison and interpretation of climate feedback processes in 19 atmospheric general circulation models. *J Geophys Res* 95:16601–16615. doi:[10.1029/JD095iD10p16601](https://doi.org/10.1029/JD095iD10p16601)
- Cess RD, Zhang MH, Ingram WJ, Potter GL, Alekseev V, Barker HW, Cohen-Solal E, Colman RA, Dazlich DA, Del Genio AD,

- Dix MR, Dymnikov V, Esch M, Fowler LD, Fraser JR, Galin V, Gates WL, Hack JJ, Kiehl JT, Le Treut H, Lo KK-W, McAvaney BJ, Meleshko VP, Morcrette JJ, Randall DA, Roeckner E, Royer JF, Schlesinger ME, Sporyshev PV, Timbal B, Volodin EM, Taylor KE, Wang W, Wetherald RT (1996) Cloud feedback in atmospheric general circulation models: an update. *J Geophys Res: Atmos* 101(D8):12791–12794. doi:[10.1029/96JD00822](https://doi.org/10.1029/96JD00822)
- Chahine MT (1993) The hydrologic cycle and its influence on climate. *Nature* 359:373–380
- Gastineau G, Li L, Le Treut H (2011) Some atmospheric processes governing the large-scale tropical circulation in idealized aquaplanet simulations. *J Atmos Sci* 68(3):553–575. doi:[10.1175/2010JAS3439.1](https://doi.org/10.1175/2010JAS3439.1)
- Gates WL (1992) AMIP: the atmospheric model intercomparison project. *Bull Am Meteorol Soc* 73(12):1962–1970. doi:[10.1175/1520-0477\(1992\)073<1962:ATAMIP>2.0.CO;2](https://doi.org/10.1175/1520-0477(1992)073<1962:ATAMIP>2.0.CO;2)
- Gent PR, Danabasoglu G, Donner LJ, Holland MM, Hunke EC, Jayne SR, Lawrence DM, Neale RB, Rasch PJ, Vertenstein M, Worley PH, Yang ZL, Zhang M (2011) The community climate system model version 4. *J Clim* 24(19):4973–4991. doi:[10.1175/2011JCLI4083.1](https://doi.org/10.1175/2011JCLI4083.1)
- Gregory J, Webb M (2008) Tropospheric adjustment induces a cloud component in CO₂ forcing. *J Clim* 21(1):58–71. doi:[10.1175/2007JCLI1834.1](https://doi.org/10.1175/2007JCLI1834.1)
- Gregory JM, Ingram WJ, Palmer MA, Jones GS, Stott PA, Thorpe RB, Lowe JA, Johns TC, Williams KD (2004) A new method for diagnosing radiative forcing and climate sensitivity. *Geophys Res Lett* 31(3):L03205. doi:[10.1029/2003GL018747](https://doi.org/10.1029/2003GL018747)
- Hansen J, Sato M, Nazarenko L, Ruedy R, Lacis A, Koch D, Tegen I, Hall T, Shindell D, Santer B, Stone P, Novakov T, Thomason L, Wang R, Wang J, Jacob D, Hollandsworth S, Bishop L, Logan J, Thompson A, Stolarski R, Lean J, Willson R, Levitus S, Antonov J, Rayner N, Parker D, Christy J (2002) Climate forcings in Goddard Institute for Space Studies SI2000 simulations. *J Geophys Res: Atmos* 107(D18):4347. doi:[10.1029/2001JD001143](https://doi.org/10.1029/2001JD001143)
- Held IM, Soden BJ (2006) Robust responses of the hydrological cycle to global warming. *J Clim* 19(21):5686–5699. doi:[10.1175/JCLI3990.1](https://doi.org/10.1175/JCLI3990.1)
- IPCC (2013) Climate change 2013: the physical science basis. Contribution of Working Group I to the 5th assessment report of the intergovernmental panel on climate change. Cambridge University Press, Cambridge, United Kingdom and New York, NY, USA
- Kamae Y, Watanabe M (2012) On the robustness of tropospheric adjustment in CMIP5 models. *Geophys Res Lett* 39(23):L23808. doi:[10.1029/2012GL054275](https://doi.org/10.1029/2012GL054275)
- Kang SM, Frierson DMW, Held IM (2009) The tropical response to extratropical thermal forcing in an idealized GCM: the importance of radiative feedbacks and convective parameterization. *J Atmos Sci* 66(9):2812–2827. doi:[10.1175/2009JAS2924.1](https://doi.org/10.1175/2009JAS2924.1)
- Kidston J, Gerber EP (2010) Intermodel variability of the poleward shift of the austral jet stream in the CMIP3 integrations linked to biases in 20th century climatology. *Geophys Res Lett* 37(9). doi:[10.1029/2010GL042873](https://doi.org/10.1029/2010GL042873)
- Klein SA, Hartmann DL (1993) The seasonal cycle of low stratiform clouds. *J Clim* 6:1587–1606
- Lin P, Yu Y, Liu H (2013) Long-term stability and oceanic mean state simulated by the coupled model FGOALS-s2. *Adv Atmos Sci* 30(1):175–192. doi:[10.1007/s00376-012-2042-7](https://doi.org/10.1007/s00376-012-2042-7)
- Lu J, Chen G, Frierson DMW (2010) The position of the midlatitude storm track and eddy-driven westerlies in aquaplanet AGCMs. *J Atmos Sci* 67(12):3984–4000. doi:[10.1175/2010JAS3477.1](https://doi.org/10.1175/2010JAS3477.1)
- Lucas C, Timbal B, Nguyen H (2014) The expanding tropics: a critical assessment of the observational and modeling studies. *Wiley Interdiscip Rev: Clim Chang* 5(1):89–112. doi:[10.1002/wcc.251](https://doi.org/10.1002/wcc.251)
- Medeiros B, Stevens B (2011) Revealing differences in GCM representations of low clouds. *Clim Dyn* 36(1):385–399. doi:[10.1007/s00382-009-0694-5](https://doi.org/10.1007/s00382-009-0694-5)
- Medeiros B, Stevens B, Held IM, Zhao M, Williamson DL, Olson JG, Bretherton CS (2008) Aquaplanets, climate sensitivity, and low clouds. *J Clim* 21(19):4974–4991. doi:[10.1175/2008JCLI1995.1](https://doi.org/10.1175/2008JCLI1995.1)
- Mitchell JFB, Wilson CA, Cunningham WM (1987) On CO₂ climate sensitivity and model dependence of results. *Q J R Meteorol Soc* 113(475):293–322. doi:[10.1002/qj.49711347517](https://doi.org/10.1002/qj.49711347517)
- Moebis B, Stevens B (2012) Factors controlling the position of the inter-tropical convergence zone on an aquaplanet. *J Adv Model Earth Syst*. doi:[10.1029/2012MS000199](https://doi.org/10.1029/2012MS000199)
- Nam C, Bony S, Dufresne JL, Chepfer H (2012) The ‘too few, too bright’ tropical low-cloud problem in CMIP5 models. *Geophys Res Lett* 39(21):L21801. doi:[10.1029/2012GL053421](https://doi.org/10.1029/2012GL053421)
- NCL (2012) The NCAR command language (version 6.1.0) [Software]. UCAR/NCAR/CISL/VETS, Boulder, Colorado. doi:[10.5065/D6WD3XH5](https://doi.org/10.5065/D6WD3XH5)
- Neale RB, Hoskins BJ (2000) A standard test for AGCMs including their physical parametrizations: I: the proposal. *Atmos Sci Lett* 1(2):101–107. doi:[10.1006/asle.2000.0022](https://doi.org/10.1006/asle.2000.0022)
- Oueslati B, Bellon G (2013) Convective entrainment and large-scale organization of tropical precipitation: sensitivity of the CNRM-CM5 hierarchy of models. *J Clim* 26(9):2931–2946. doi:[10.1175/JCLI-D-12-00314.1](https://doi.org/10.1175/JCLI-D-12-00314.1)
- Raper SCB, Gregory JM, Stouffer RJ (2002) The role of climate sensitivity and ocean heat uptake on AOGCM transient temperature response. *J Clim* 15(1):124–130. doi:[10.1175/1520-0442\(2002\)015<0124:TROCSA>2.0.CO;2](https://doi.org/10.1175/1520-0442(2002)015<0124:TROCSA>2.0.CO;2)
- Rose BEJ, Armour KC, Battisti DS, Feldt N, Koll DDB (2014) The dependence of transient climate sensitivity and radiative feedbacks on the spatial pattern of ocean heat uptake. *Geophys Res Lett* 41(3):1071–1078. doi:[10.1002/2013GL058955](https://doi.org/10.1002/2013GL058955)
- Satoh M, Matsuno T, Tomita H, Miura H, Nasuno T, Iga S (2008) Nonhydrostatic icosahedral atmospheric model (NICAM) for global cloud resolving simulations. *J Comput Phys* 227(7):3486–3514. doi:[10.1016/j.jcp.2007.02.006](https://doi.org/10.1016/j.jcp.2007.02.006)
- Shine KP, Cook J, Highwood EJ, Joshi MM (2003) An alternative to radiative forcing for estimating the relative importance of climate change mechanisms. *Geophys Res Lett* 30(20):2047. doi:[10.1029/2003GL018141](https://doi.org/10.1029/2003GL018141)
- Slingo JM (1987) The development and verification of a cloud prediction scheme for the ECMWF model. *Q J Roy Meteorol Soc* 113:899–927
- Soden BJ, Broccoli AJ, Hemler RS (2004) On the use of cloud forcing to estimate cloud feedback. *J Clim* 17(19):3661–3665
- Stevens B, Bony S (2013) What are climate models missing? *Science* 340(6136):1053–1054. doi:[10.1126/science.1237554](https://doi.org/10.1126/science.1237554)
- Stevens B, Giorgetta M, Esch M, Mauritsen T, Crueger T, Rast S, Salzmann M, Schmidt H, Bader J, Block K, Brokopf R, Fast I, Kinne S, Kornbluh L, Lohmann U, Pincus R, Reichler T, Roeckner E (2013) Atmospheric component of the MPI-M Earth system model: ECHAM6. *J Adv Model Earth Syst* 5(2):146–172. doi:[10.1002/jame.20015](https://doi.org/10.1002/jame.20015)
- Tiedtke M (1993) Representation of clouds in large-scale models. *Mon Wea Rev* 121(11):3040–3061
- Tomassini L, Geoffroy O, Dufresne JL, Idelkadi A, Cagnazzo C, Block K, Mauritsen T, Giorgetta M, Quaas J (2013) The respective roles of surface temperature driven feedbacks and tropospheric adjustment to CO₂ in CMIP5 transient climate simulations. *Clim Dyn* 1–24. doi:[10.1007/s00382-013-1682-3](https://doi.org/10.1007/s00382-013-1682-3)
- Vial J, Dufresne JL, Bony S (2013) On the interpretation of inter-model spread in CMIP5 climate sensitivity estimates. *Clim Dyn* 1–24. doi:[10.1007/s00382-013-1725-9](https://doi.org/10.1007/s00382-013-1725-9)

- Voldoire A, Sanchez-Gomez E, Salas y Mélia D, Decharme B, Cassou C, Sénési S, Valcke S, Beau I, Alias A, Chevallier M, Déqué M, Deshayes J, Douville H, Fernandez E, Madec G, Maisonnave E, Moine MP, Planton S, Saint-Martin D, Szopa S, Tyteca S, Alkama R, Belamari S, Braun A, Coquart L, Chauvin F (2012) The CNRM-CM5.1 global climate model: description and basic evaluation. *Clim Dyn* 1–31. doi:[10.1007/s00382-011-1259-y](https://doi.org/10.1007/s00382-011-1259-y)
- Watanabe M, Suzuki T, O'ishi R, Komuro Y, Watanabe S, Emori S, Takemura T, Chikira M, Ogura T, Sekiguchi M, Takata K, Yamazaki D, Yokohata T, Nozawa T, Hasumi H, Tatebe H, Kimoto M (2010) Improved climate simulation by MIROC5: mean states, variability, and climate sensitivity. *J Clim* 23(23):6312–6335. doi:[10.1175/2010JCLI3679.1](https://doi.org/10.1175/2010JCLI3679.1)
- Williamson D, Blackburn M, Hoskins B, Nakajima K, Ohfuchi W, Takahashi Y, Hayashi YY, Nakamura H, Ishiwatari M, McGregor J, Borth H, Wirth V, Frank H, Bechtold P, Wedi N, Tomita H, Satoh M, Zhao M, Held I, Suarez M, Lee MI, Watanabe M, Kimoto M, Liu Y, Wang Z, Molod A, Rajendran K, Kitoh A, Stratton R (2012) The APE Atlas. Technical report. National Center for Atmospheric Research, doi:[10.5065/D6FF3QBR](https://doi.org/10.5065/D6FF3QBR)
- Winton M, Takahashi K, Held IM (2010) Importance of ocean heat uptake efficacy to transient climate change. *J Clim* 23(9):2333–2344. doi:[10.1175/2009JCLI3139.1](https://doi.org/10.1175/2009JCLI3139.1)
- Wyant MC, Bretherton CS, Blossey PN (2012) Fast cloud adjustment to increasing CO₂ in a superparameterized climate model. *J Adv Model Earth Syst* 4:M05001. doi:[10.1029/2011MS000092](https://doi.org/10.1029/2011MS000092)
- Yoshizaki M, Si Iga, Satoh M (2012) Eastward-propagating property of large-scale precipitation systems simulated in the coarse-resolution NICAM and an explanation of its appearance. *SOLA* 8:21–24. doi:[10.2151/sola.2012-006](https://doi.org/10.2151/sola.2012-006)
- Yukimoto S, Adachi Y, Hosaka M, Sakami T, Yoshimura H, Hirabara M, Tanaka TY, Shindo E, Tsujino H, Deushi M, Mizuta R, Yabu S, Obata A, Nakano H, Koshiro T, Ose T (2012) A new global climate model of the Meteorological Research Institute: MRI-CGCM3—model description and basic performance—. *J Meteorol Soc Jpn Ser II* 90A:23–64. doi:[10.2151/jmsj.2012-A02](https://doi.org/10.2151/jmsj.2012-A02)
- Zelinka MD, Klein SA, Taylor KE, Andrews T, Webb MJ, Gregory JM, Forster PM (2013) Contributions of different cloud types to feedbacks and rapid adjustments in CMIP5. *J Clim* doi:[10.1175/JCLI-D-12-00555.1](https://doi.org/10.1175/JCLI-D-12-00555.1)